Structures 51 (2023) 105–123

Contents lists available at ScienceDirect

Structures

journal homepage: www.elsevier.com/locate/structures

Quantifying the effect of amplitude scaling of real ground motions based on structural responses of vertically irregular and regular RC frames

Mehmet Palanci [a,*], Ahmet Demir [b], Ali Haydar Kayhan [c]

[a] Department of Civil Engineering, Istanbul Arel University, Istanbul, Turkey
[b] Department of Civil Engineering, Bolu Abant Izzet Baysal University, Bolu, Turkey
[c] Department of Civil Engineering, Pamukkale University, Denizli, Turkey

ARTICLE INFO

Keywords:
Scaling factor
Seismic codes
Real ground motion selection
Ground motion parameters
Dynamic analysis

ABSTRACT

Increasing number of real ground motion (GM) record databases raised nonlinear dynamic analysis (NDA) as an attractive option to determine structural response statistics. Structural responses are sensitive to input motions and the appropriate selection and scaling of real GMs is one of the crucial topics in earthquake engineering. In this paper, the influence of amplitude scaling on important earthquake demand parameters (EDPs), namely, global drift ratio, inter-story drift ratio and maximum floor acceleration, were studied using different scaling approaches and scaling limits. Eurocode-8 was used as a reference seismic code and amplitude scaling effects on structural responses of vertically irregular and regular structures were quantified. Efficiency and sufficiency of amplitude scaling were assessed in terms of mean, dispersion and non-exceedance probability curves of the EDPs. Statistical distribution of GM characteristics and their dependence on GM amplitude scaling were also discussed. Evaluations have shown that similar mean responses can be obtained regardless of scaling limits, approaches, and building topology if spectral shape compatibility is ensured. Furthermore, results demonstrated that neither building regularity nor scaling of GMs influenced the statistical distribution of ground motion parameters and non-exceedance probability curves of the EDPs. In fact, it was revealed that record selection scenario including spectral compatibility of individual GMs had a dramatic impact on dispersion and exceedance probability of structural responses.

1. Introduction

NDA is a compelling instrument to determine seismic capacity and EDPs of structures and infrastructures by utilizing the set of GM records as input. This tool is mostly preferred by modern seismic codes also [1–3] and GM records are selected by spectral ordinate matching of input GMs with target spectrum which is mostly described as uniform hazard spectrum. Basically, three options such as artificial, simulated/synthetic and real GMs are available for practitioners to obtain GM records to match target spectrum. Real GMs are mostly preferred since they are free from the problems associated with simplifications and assumptions made and they do not need the special engineering seismologist service. Furthermore, a considerable number of real GMs can easily be accessed through many GM databases on the internet [4–6].

The utmost challenging issue obstructing the use of real GM records for NDA is the appropriate selection and scaling of GM records. Soil condition, target spectrum, moment magnitude and source-to-site distance (M_w–R) pairs based on the seismicity of construction region and even natural period/conditioning period affected from structural configuration are the primary sources of creating (i.e., pre-selection) input GM sets. Distinct performance objectives for different seismic hazard levels also increase the complexity and GM scaling becomes an alternative option to solve spectral matching-based record selection problem. To overcome such an overwhelming issue, various tools and record selection frameworks have been improved until recently [7–12]. Despite improvements in GM selection methods in earthquake engineering, scaling values recommended for real GMs can be varied. Several studies examined only the scaling values larger than unity [13,14] while others concentrated on different scaling value range(s)/bin(s) smaller or larger than unity [15–19]. Global/inter-story displacement/drift ratio demands, and the dependency of GM parameters (referred as intensity measures (IMs) in this study hereafter) were commonly evaluated using different building types and selection methods. Furthermore, structural response bias between unscaled and

* Corresponding author.
E-mail addresses: mehmetpalanci@arel.edu.tr (M. Palanci), ahmetdemir@ibu.edu.tr (A. Demir), hkayhan@pau.edu.tr (A.H. Kayhan).

https://doi.org/10.1016/j.istruc.2023.03.040
Received 5 October 2022; Received in revised form 9 December 2022; Accepted 7 March 2023
Available online 14 March 2023

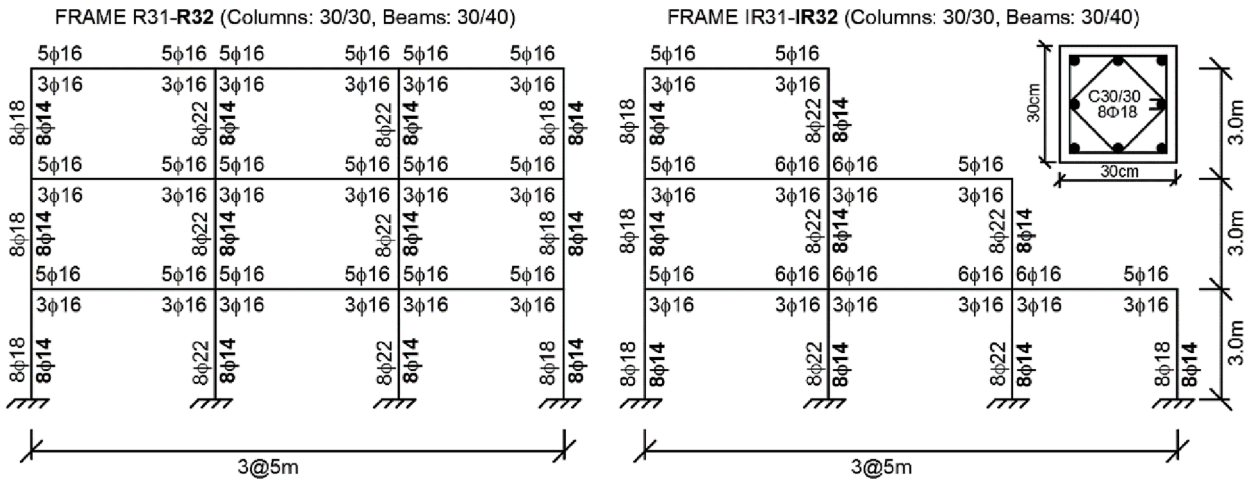

Fig. 1. Geometrical and reinforcement details of R3 and IR3 frames.

scaled GM records were used to investigate scaling effects in these studies [13–15,17,18] and unscaled sets were used as targets since they were represented as a particular seismic event or scenario. On the other hand, unscaled GM record sets can be highly dispersed [20], questioning whether selected sets can be really considered as targets. Therefore, a bias between the unscaled and scaled GMs might be controversial from a seismic code perspective. Nevertheless, the influence of scaling of real GMs on the response of structures is still disputed since acceptable GM scaling limits are wide from unity to 10 or more. Some studies about the selection and scaling stated that bias in structural responses resulted

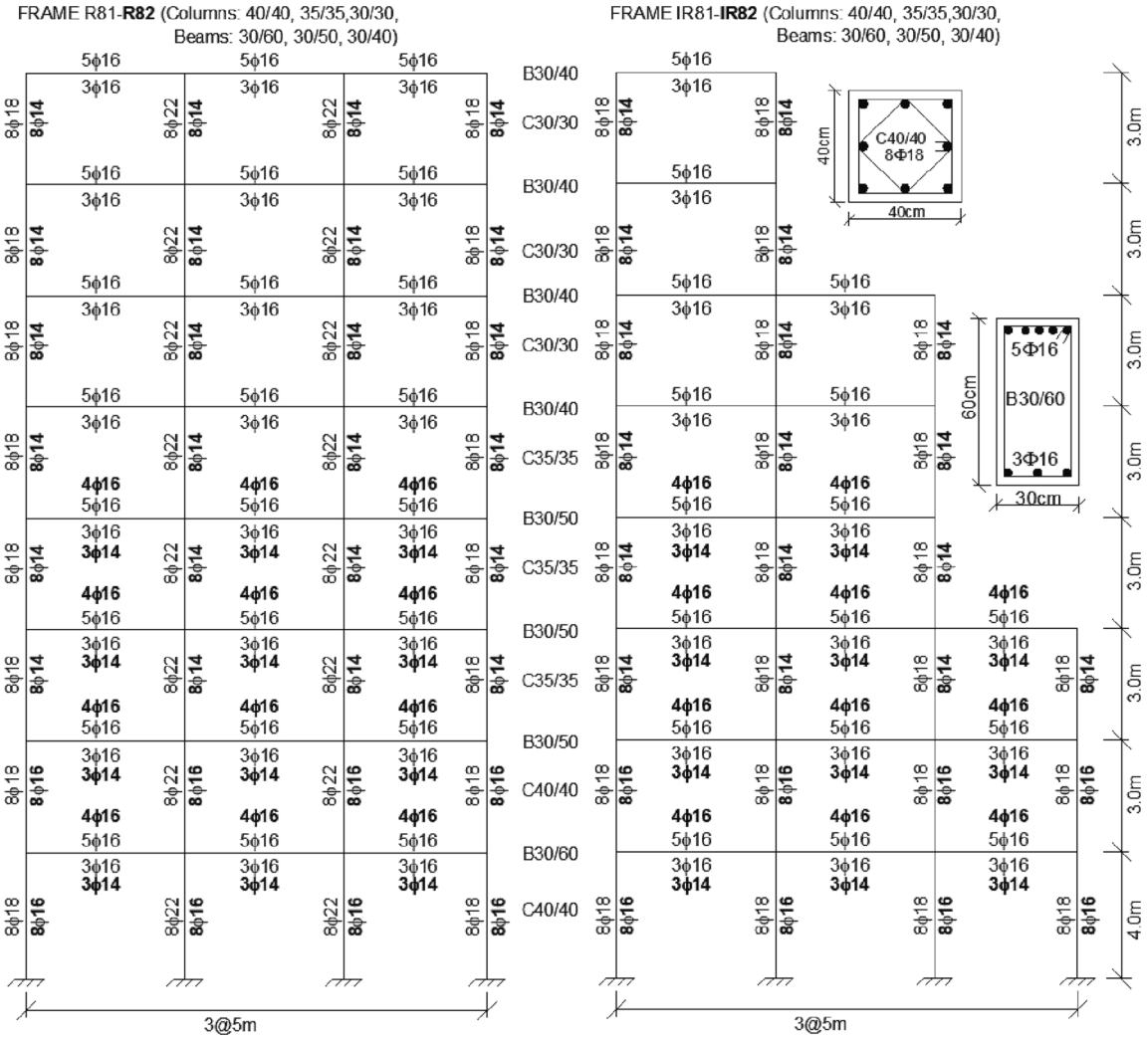

Fig. 2. Geometrical and reinforcement details of R8 and IR8 frames.

Table 1
Section dimensions and reinforcement details of all frames used in the study.

Story	Section dimensions		Reinforcement details	
	Column (cm)	Beam (cm)	Column	Beam
	3-Story (8-Story)	3-Story (8-Story)	3-Story (8-Story)	3-Story (8-Story)
1st	30x30 (40x40)	30x40 (30x60)	8ϕ14-8 ϕ 18–8 ϕ 22	Top:5 ϕ 16–6 ϕ 16; Bottom:3 ϕ 16
2nd	30x30 (40x40)	30x40 (30x50)	(8 ϕ 14–8 ϕ 16–8 ϕ 18–8 ϕ 22)	(Top:5 ϕ 16–4 ϕ 16; Bottom:3 ϕ 16–3 ϕ14)
3rd	30x30 (35x35)	30x40 (30x50)		
4th	(35x35)	(30x50)	(8 ϕ 14–8 ϕ 16–8 ϕ 18–8 ϕ 22)	(Top:5 ϕ 16–6 ϕ 16- Bottom:3 ϕ 16)
5th	(35x35)	(30x40)		
6th	(30x30)	(30x40)		(Top:5 ϕ 16–4 ϕ 16- Bottom:3 ϕ 16–3 ϕ 14)
7th	(30x30)	(30x40)		
8th	(30x30)	(30x40)		

from the spectral shape difference and could be precluded if spectral shape compatibility [18,21–23] is ensured. On the other hand, these studies mainly rely on the seismic hazard analysis (SHA) framework, first-mode-dominated or conditioned period structures and have no numerical assessment of differences within selected records. Despite the all progresses, it can be said that studies on appropriate scaling of real GMs including code-based record selection considering spectral compatibility are limited.

The purpose of this study is to assess structural response statistics of multi degree of freedom models (MDOF) in code-based and probabilistic respect, using different scaling approaches and scaling limits including spectral shape compatibility of individual GMs. In addition, effect of amplitude scaling on the distribution of various IMs such as peak ground velocity (*PGV*), arias intensity (*AI*), significant duration (*SD*), cumulative absolute velocity (*CAV*) and Housner Intensity (*HI*) that represent the different GM characteristics, were also assessed. Eurocode-8 [1] was used as reference seismic code, two distinct three- and eight-story reinforced concrete (RC) building frames and their vertically irregular topologies representing the modern and old design practices of Europe were employed. Stochastic spreadsheet software tool, SpeCRS [12], was used to select GMs and differences within the selected records were quantified. The effect of amplitude scaling was inspected using mean and dispersion considering the global drift ratio, inter-story drift ratio and for the first time, maximum floor acceleration (*MFA*). Not only structural responses were quantified but also plastic hinge formation of building frames was compared and discussed under different scaling approaches. In addition, a generalized conditional intensity measure (GCIM) method [24] under scenario-earthquake was used to evaluate the sufficiency of selected GMs and to investigate their dependency to scaling limits and approaches for concerning IMs. Non-exceedance probability curves adopted in FEMA P-58 [25] regarding EDPs were also calculated and compared. Consequently, general remarks and implications were summarized.

2. Structural analysis models

In this study, two different structural frame typologies classified as vertically regular and irregular frames were used. In addition to structural typologies, story numbers of buildings were different, and three and eight story RC frames were selected to represent the low- and medium-rise buildings. Furthermore, these frames were grouped according to their design procedure. The first group of frames were entitled as R31, IR31, R81 and IR81. They consist of four typical beam–column frame buildings without shear walls, located in a high-seismic region of Europe considering both gravity and seismic loads. During the seismic design of these buildings, peak ground acceleration (*PGA*) was taken as 0.2 g and it was assumed that buildings were constructed on local soil class B according to Eurocode-8. The second group of frames were only designed by gravity loads and they were named as R32, IR32, R82 and IR82 regarding most of the existing RC buildings that were designed by early seismic provisions without application of a lateral load pattern. It is worth noting that both structural groups have the same geometry and vertical loads, but they have different reinforcement details. Both frames were designed by Hatzigeorgiou and Liolios [26] and further details for the frames can be read in the related study.

Some important attributes of buildings such as span length, story height, member (columns and beams) dimensions and reinforcement details of the members are illustrated in Figs. 1 and 2. The total length of the frames is 15 m (3 × 5 m). Building height is 9 m for three-story frames while 25 m for eight-story frames. Section dimensions and reinforcement details of the members are provided in Table 1 for each story. In the table, the values outside and inside the parentheses are about three- and eight-story buildings, respectively. It can be seen from Table 1 that all columns are in square dimensions and dimensions of columns were reduced in upper stories for eight-story building frames. Reinforcement details of the members given in Table 1 are also shown in Figs. 1 and 2, and the details of R32, R82, IR32 and IR82 frames are shown in bold to avoid repetitions. For sake of simplicity, reinforcement details of columns are just given in the middle, but reinforcement details of both sides (left and right) of the beams are the same.

Unconfined concrete compressive strength (f_c) was presumed as 20 MPa and yield strength (f_y) of longitudinal and transverse reinforcement was taken as 500 MPa. Dead and live loads were taken as 20 kN/m and 10 kN/m for beams, respectively. Just vertical loads of concrete slabs were considered, and calculated loads were assigned to the beams. All considered building frames were modeled for nonlinear dynamic analysis accounting for the abovementioned loading (dead, live and self-weight) conditions, reinforcing details and cross-sectional dimensions of members. Nonlinear static and dynamic analyses were conducted by SAP2000 [27]. Using the cross-sectional dimensions, materials [26] and axial loads for the members, strength and deformation capacity of the members were obtained by conducting moment–curvature analyses. Bilinearized moment–curvature response of the members was converted to moment-plastic rotation curves, and lumped plastic hinges were assigned to critical regions of the members where the damage was expected to occur. Plastic hinge length was taken as half of section depth. Details about the determination of member deformation capacities and

Table 2
Some structural characteristics of the frames.

RC Frames	H (m)	T_1 (s)	T_2 (s)	T_3 (s)	α_1	α_2	α_3	*Sum of* α_i	V_t/W (%)	W (kN)
R31	9.0	0.611	0.189	0.107	0.866	0.107	0.027	1.000	40.0	1035.0
IR31	9.0	0.470	0.190	0.118	0.799	0.160	0.041	1.000	59.0	690.0
R81	25.0	1.220	0.453	0.253	0.773	0.145	0.043	0.961	17.0	2760.0
IR81	25.0	0.955	0.430	0.266	0.689	0.199	0.058	0.946	22.0	1955.0
R32	9.0	0.611	0.189	0.107	0.866	0.107	0.027	1.000	29.0	1035.0
IR32	9.0	0.470	0.190	0.118	0.799	0.160	0.041	1.000	38.0	690.0
R82	25.0	1.220	0.453	0.253	0.773	0.145	0.043	0.961	13.0	2760.0
IR82	25.0	0.955	0.430	0.266	0.689	0.199	0.058	0.946	17.0	1955.0

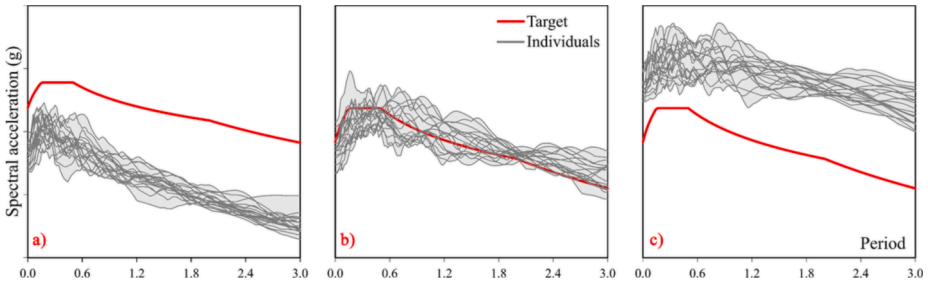

Fig. 3. Examples about target spectrum and possible individual spectra of GMs in a GM catalog.

bilinearization procedure are provided by Palanci [28]. Other damage levels such as immediate occupancy (IO) and life safety (LS) were determined assuming 10% and 75% of plastic hinge deformation capacity, respectively.

In Table 2, calculated dynamic characteristics of frames; natural vibration period (T) and modal participating mass ratio (α) of first three periods are given. In addition, lateral strength capacity ratio (V_t/W) determined from pushover analysis, building height (H) and seismic weight (W) of the frames are provided in the table. As can be seen, the periods of R31 and R32 are equal since both frames have the same geometry and section dimensions. Sum of first three modal participating mass ratios for three-story frames is slightly higher than that for eight-story frames. It can also be said that lateral strength capacity ratio (V_t/W) of three-story frames higher than eight-story ones. It can also be observed that R32, IR32, R82 and IR82 have smaller V_t/W values than R31, IR31, R81 and IR81 owing to lower amount of longitudinal reinforcement ratios.

3. Background for selection and scaling of real ground motion records

The first selection (can be called pre-selection) of GM records for the sake of design or performance determination of buildings begins with the determination of candidate GM suites. Thus, a GM catalog of pre-selected records is created and used for the selection of appropriate GM records. This step has a crucial role for the whole selection procedure, and it may rely on many circumstances such as geotechnical issues related to soil conditions, seismicity of the region, restrictions in record selection, target spectrum and even structural configuration which affect the structural period and hence the selection procedure. Seismicity, soil conditions and target spectrum among them have utmost importance since they play a key role in creating a GM catalog. Depending on the seismicity of the region and soil conditions, pre-selected records may not be perfectly compatible with the target spectrum. Accordingly, pre-selected records may be either lower or higher than the target spectrum as shown in Fig. 3a and Fig. 3c. This situation will clearly affect the scaling of GM records to match the target spectrum and a gap between the target spectrum and pre-selected records may dramatically increase scaling value (SV) and vice versa. On the other hand, despite the many challenging issues, pre-selected records and target spectrum may be suitable (see Fig. 3b) and it will ease record selection, and scaling values will be around unity. Even under such circumstance, the use of different seismic intensity levels for the distinct performance objectives in the design or performance evaluation of structures may result unfavorable conditions since there is a risk of opening gap between the target spectrum and the spectra of pre-selected records (as observed in Fig. 3a and 3c) according to the desired level of earthquake intensity level.

Table 3
Scaling value range for approaches A and B.

Case	Approach A	Approach B
1	SV = 1.00	1.00 < SV < 4.00
2	0.50 < SV < 2.00	4.00 < SV < 8.00
3	0.25 < SV < 4.00	8.00 < SV < 12.00
4	0.10 < SV < 10.00	12.00 < SV < 16.00
5	0.05 < SV < 20.00	16.05 < SV < 20.00

According to the possible conditions and mandatory circumstances, extremely low or high SVs may be observed and extreme values for record selection may be evaluated as inconvenient and not reliable for the analysis [13,14,18]. To assess the effects of such cases on the seismic demand and behavior of structures, different selection scenarios, scaling approaches and scaling cases were examined. GM selection considering only mean spectrum of selected GMs for compatibility with the target spectrum is the first scenario. Considering compatibility between both individual spectra of selected GMs and their mean spectrum with the target spectrum is the second scenario. Two different approaches were used for the first scenario (A and B) and second scenario (C and D), separately. Thus, four approaches named as A, B, C and D based on the selecting and scaling of GMs were used. To obtain the required compatibility with the target spectrum (i.e., to minimize the shaded area in Fig. 4b), SVs used for GM records may be bigger or smaller than unity. In Fig. 4a, the acceleration spectrum of an original individual record spectrum and two scaled forms of the spectrum were given as examples.

A and B approaches consider only matching of mean spectrum of selected GMs with target spectrum in the period range of [0.2 T – 2.0 T] as recommended in Eurocode-8. These approaches are distinguished by

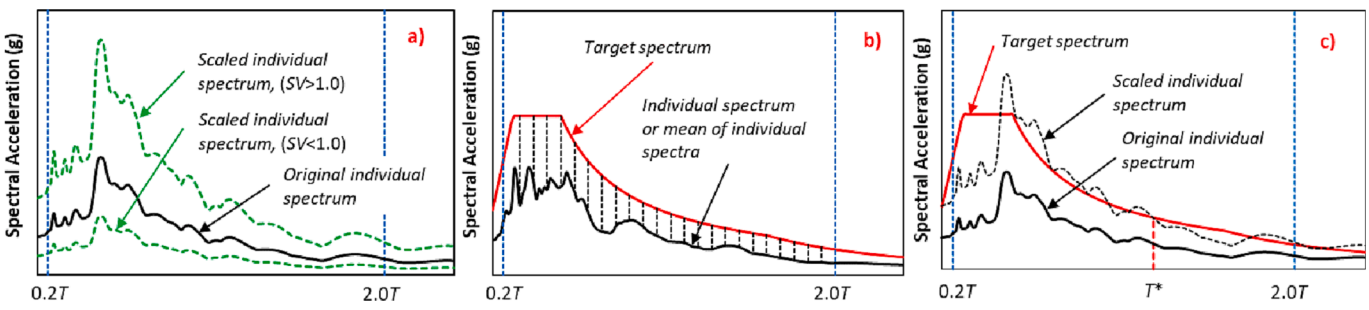

Fig. 4. Selection scenarios and scaling approaches used in this study.

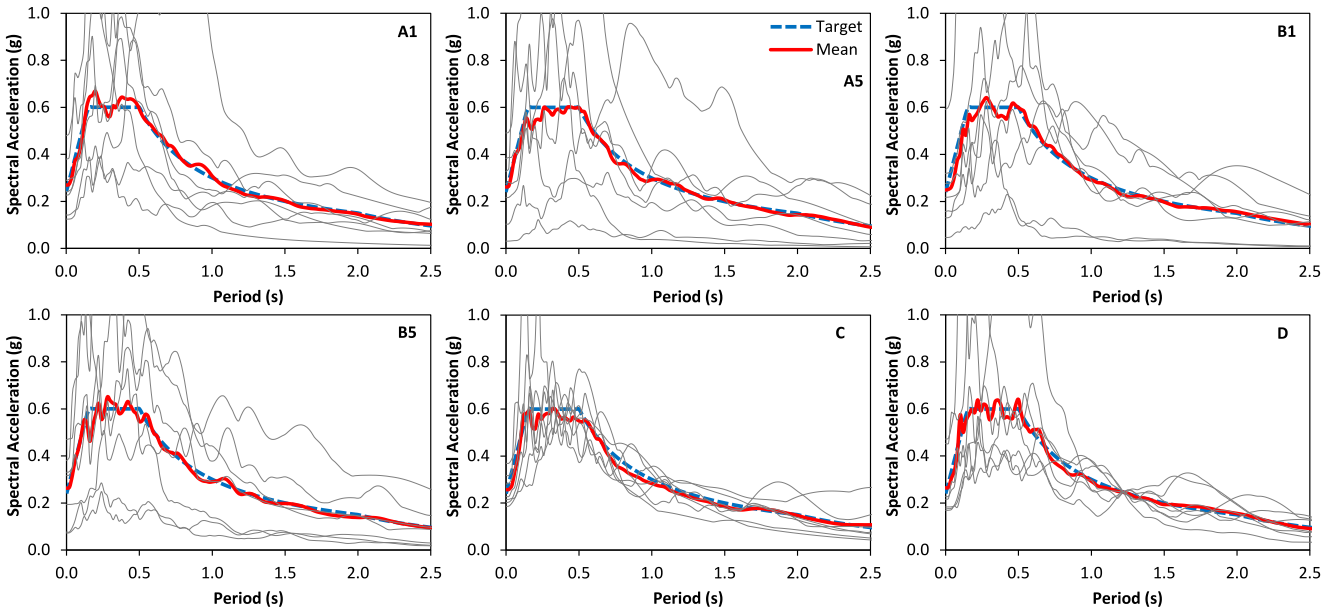

Fig. 5. Mean and individuals spectra for R81 determined from different approaches in the study.

using different scaling cases based on SV range. SVs for approach A can be equal, lower or even higher than unity. For example, SV for A1 approach is equal to unity, which means that original (unscaled) GM records are used while scaling range is between 0.50 and 2.00 for A2 approach. It can be seen in Table 3 that five different cases were considered for A and B approaches. Scaling range gets wider in approach A with increasing case number such as scaling range for A3 is 0.25–4.00 while this range is 0.05–20.00 for A5 approach. The other scaling approach B has also five different cases, but scaling ranges were taken constant in all cases. However, compared to approach A, scaling ranges in B approaches were always greater than unity and were used to evaluate the use of extremely high SVs.

In addition to compatibility between mean and target spectrum, compatibility of individual spectra with target spectrum is considered by C and D approaches. For approach C, spectral compatibility for both individual spectra and their mean are considered in the period range of 0.2 T-2.0 T simultaneously. Accordingly, each GM in the catalog is first multiplied with SV_{C1}. SV_{C1} is the coefficient which is used to minimize shaded area between target spectrum and individual spectra of GMs in the catalog as shown in Fig. 4b. Then, each GM is modified by SV_{C2} (between 0.90 and 1.10) to obtain better compatibility between the mean spectrum and target spectrum [20]. It should be noted that SV_{C1} and SV_{C2} can be different for a GM record from other records. Consequently, $SV_C = SV_{C1}{*}SV_{C2}$ is used for each GM record. D approach, on the other hand, is strictly constraint to match the target spectrum at T^* which can be considered as the natural period of building in the direction of earthquake excitation. Thus, SV_D for each GM record is determined by $S_{ae}(T^*)/S_a(T^*)$ and spectral value of scaled GM and target spectrum is equal at T^* (Fig. 4c). In both scaling approaches, SV ranges were kept wide and between 0.05 and 20.00 since different restrictions were considered for record selection. It can be admitted that variation of spectral acceleration values for the period of interest will be considerably lower than A and B approaches due to special consideration of individual spectra. Numerical evaluations based on record selection scenarios and scaling approaches are given in the next section.

In summary, approach A gathers the different characteristics of GM records which have the acceleration spectra below and above the target spectrum by wide range of SVs while approach B only adopts the GMs records relatively lower spectra with respect to target spectrum. Both approaches are the exact applications of Eurocode-8 rules. In addition to code practices, C and D approaches consider a scenario about individual spectra for better spectral shape compatibility. For each of the record scaling approaches and cases, ten record sets consisting of seven GM records were obtained, separately. For instance, 70 GM records (multiplication of 10 sets and 7 records) were used for just A1, and structural responses were determined using these records. The GM record sets of other scaling approaches and cases for each building frame were similarly obtained and used for the analyses. Spectral shape compatibility is formulated as an engineering optimization problem to select and scale GM records for each scenario and approach from the created GM catalog. Stochastic harmony search optimization-based solution algorithm was used [12,29,30].

PEER strong-motion database [6] was used to create a GM catalog by pre-selection of real GM records. Three different criteria were used for pre-selection. First, earthquake magnitude (M_w) was taken equal or greater than 5.0. Second, the epicentral distance to the recorded station of GM (R) was between 10 and 60 km. Third, shear wave velocity (V_{s30}) was between 360 and 800 m/s to account design soil type (i.e., soil class B) according to Eurocode-8. Totally, 2106 horizontal components of 1053 GM records were selected from the database considering the criteria. It should be noted that the criteria represent mid- and high-intensity earthquakes [29].

4. Comparison and assessment of stochastically selected real GM sets

GMs were selected for each record set using GM selection schemes given in the earlier section for each building type and approach. Individual spectra and their mean spectrum of the sample sets obtained by A1, A5, B1, B5, C and D approaches for R81 frame are plotted in Fig. 5. It can be seen from the figures that the mean spectra of selected GM records have good agreement with the target spectrum for all approaches.

If special attention is paid to the spectral shape of selected records, it can be said that spectral acceleration variation of individual records for C and D approaches is considerably lower than the other approaches and individual GMs have also good agreement with mean spectra. In addition, the spectral compatibility of D approach for individual T^* is perfectly suited to the target spectrum and the variation of spectral acceleration at T^* is equal to zero. To quantify spectral compatibility, a quantitative δ parameter [31] was used and this parameter was calculated between the mean spectrum of selected records and the target spectrum for each record set. δ is simply mean square root of the sum of

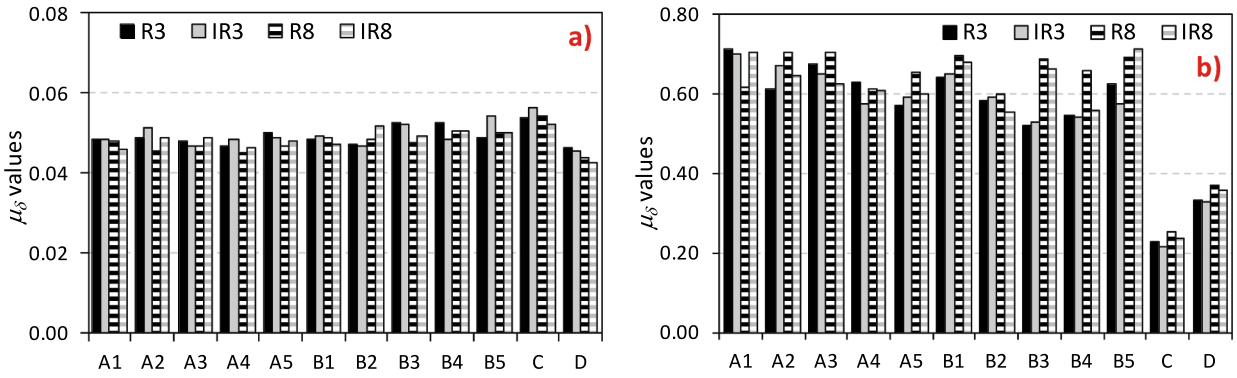

Fig. 6. μδ values for mean (a) and individuals (b) spectrum according to scaling approach.

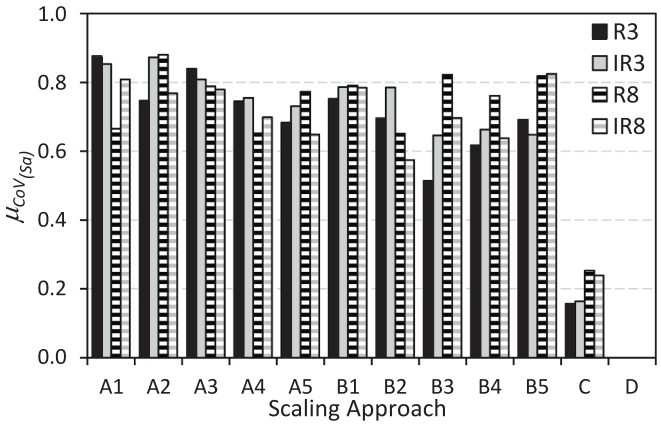

Fig. 7. $\mu_{CoV(Sa)}$ values at the first mode of the RC frames (T^*).

the squares normalized to the target spectrum in the period range of interest. Furthermore, this parameter can also be used to quantify the compatibility of individual spectra with the target spectrum as described by Demir et al. [29]. Then, the mean of ten δ values of ten different GM record sets (μδ) are calculated as the expected value of δ for a scaling approach and a frame. μ δ values for mean and individual spectra are given in Fig. 6 for all frames.

In Fig. 6a, μ_δ is almost uniform for all scaling approaches and cases, and it can be said that μ_δ values are quite low, which shows the agreement between the shape of the mean spectrum of selected records and target spectrum. Although μ_δ values clearly show a quite good agreement since they are quite lower than 0.1 [32], differences between μ_δ values of selection scenarios and scaling approaches should be quantified. To make a quantitative assessment, one-way analysis of variance (ANOVA) [33] was performed to evaluate whether differences of μ_δ values between and among the selection scenarios and scaling approaches were statistically significant. Confidence level was assumed 5% and *F*-critical value was computed as 1.88. *F*-values for R3, IR3, R8 and IR8 were obtained as 0.89, 1.14, 0.69 and 1.86, respectively. Since the *F*-values are lower than the *F*-critical value, it can be concluded that the differences between the residuals of δ between the selection scenarios and scaling approaches are statistically insignificant. Accordingly, spectral shape bias between the scaling approaches and scaling limits is negligible.

Obtained μ_δ values for individual GMs are also provided in Fig. 6b and it can be said that values for C and D approaches are considerably lower than other approaches. This situation clearly emphasizes the effect of special consideration of individual spectra during selection. It can be admitted that individual spectra are well matched with target spectrum, especially for C and D approaches while δ values calculated for mean spectrum in the period range of 0.2 *T* and 2.0 *T* are considered.

In addition to assessment of GM records for the period range of interest described in Eurocode-8, variation of spectral acceleration values around the mean at the specific period of T^* was investigated. The natural vibration period of the frames was provided in Table 2 and each frame has characteristic period values according to the table. For this reason, the coefficient of variation for S_a values ($CoV(S_a)$) was calculated for each GM record set. The mean of the $CoV(S_a)$ values ($\mu_{CoV(Sa)}$) was shown in Fig. 7 for all record sets and each frame separately. It can be observed again that $\mu_{CoV(Sa)}$ values of C and D approaches are considerably lower than A and B approaches. In fact, $\mu_{CoV(Sa)}$ for D approach is zero and it perfectly matches the target spectrum at the natural period of a frame. According to Fig. 7, $\mu_{CoV(Sa)}$ for C approach is around 0.2, while A and B approaches are higher than 0.7 on average.

Although compatibility of record sets is well, one of the intriguing questions is how SVs are affected and changed according to record selection scenario and approaches. Since each approach has its own constrains and all processes are completely stochastic, obtained SVs were random even in a set. To evaluate this issue, cumulative distribution functions (CDFs) of SVs were calculated for all frames and each case. CDF of each frame and scaling approach is distinguished to assess changes in SVs and results are plotted in Fig. 8. In the figures, CDF of A1 approach is not illustrated since CDF is constant and equal to unity due to selection of original GMs.

Fig. 8 should be read with Section 3 to understand the CDF of the scaling approaches and it can be concluded that trend of CDFs for each approach is distributed in accordance with its own rules. For example, scaling values for B4 approach are between 12 and 16 and dispersion of A5 has agreement with pre-defined scaling range. When the distribution of CDF for each frame and approach is compared, it can be assumed that distribution of CDFs of different frames are inter-correlated regardless of irregularity and/or story number. Scaling limits for A5, C and D approaches are almost identical and when the CDF of these approaches are compared, it can be admitted that CDF distribution of C and D approaches have a close relation, but CDF of A5 is not. CDF of C and D approaches more likely to parabolic curve while A5 is almost linear.

To give a different perspective for SVs during the record selection process, mean SVs of all records in the record sets were calculated and they were converted to scale factors (SFs). SF is simply the amplitude of scaled GM to original GM, and it is always greater than unity. If SV is lower than unity, the multiplicative inverse of SV is taken. Mean values of obtained SFs are plotted in Fig. 9. It can be observed from the figure that mean SV of distinct buildings are almost same for each approach.

Distribution of mean SFs for approach A is increasing more drastically compared to different cases of B approach and gradual increasing is observed in B approach. It is observed from Fig. 9 that the mean SFs for B approach are almost the medium value of the defined range in all cases. If mean SFs of C and D approaches are checked, it can be told that smaller changes are obtained for different frames and SFs are in common, and it is around four. Furthermore, SFs are almost identical, and

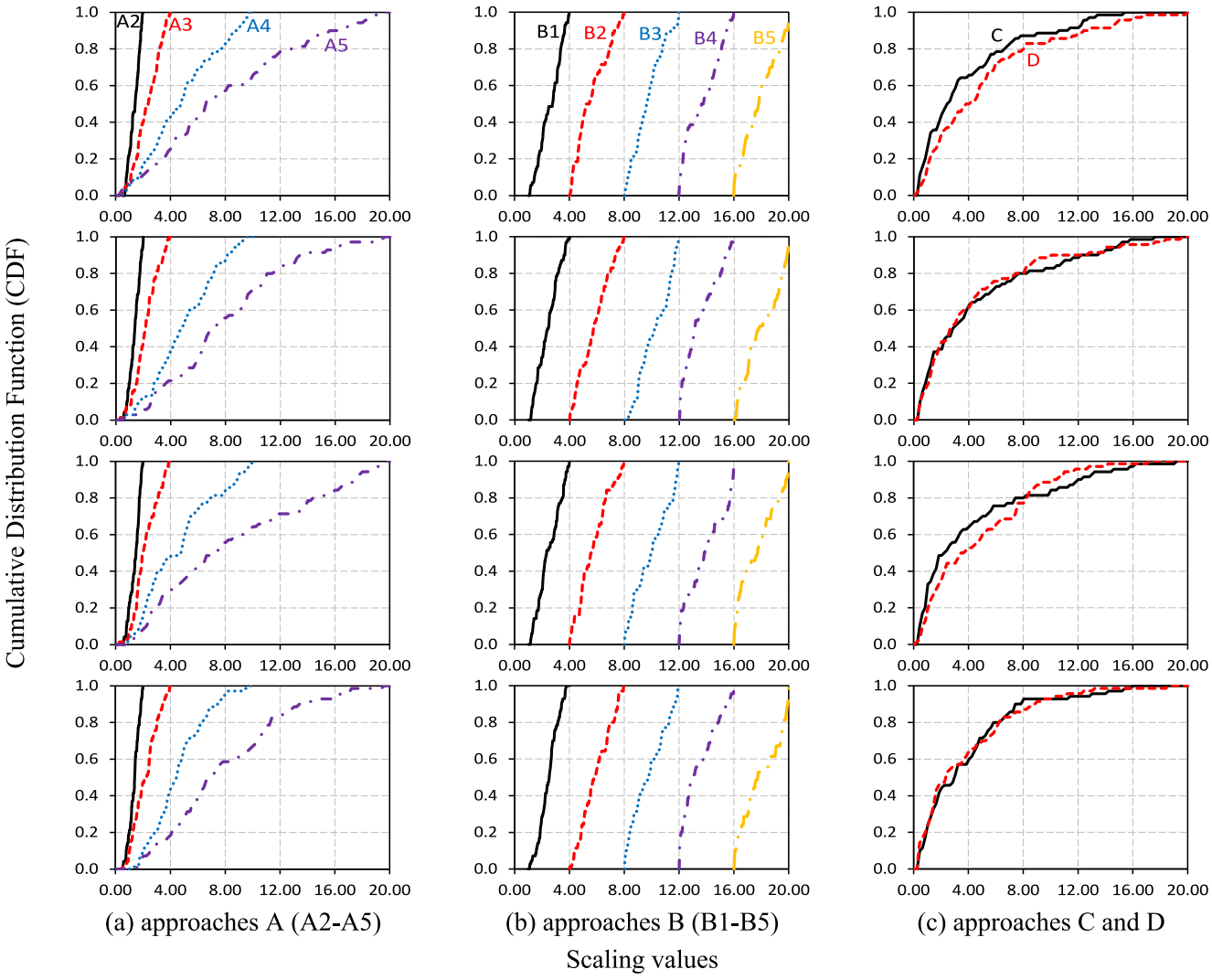

Fig. 8. Cumulative distribution function of scaling approaches for all frames (Top to bottom: R3, IR3, R8 and IR8).

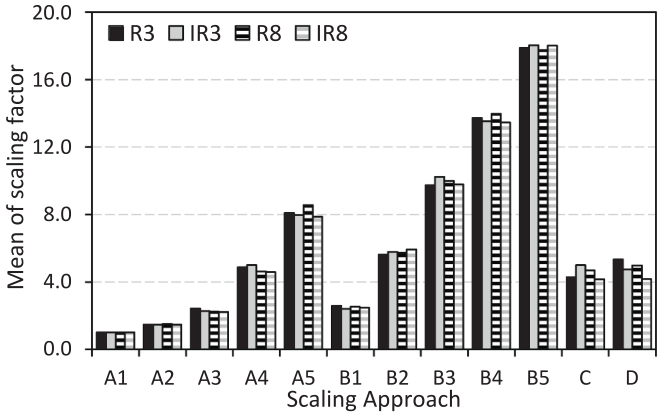

Fig. 9. Mean scaling factors for all scaling approaches and RC frames.

they do not vary dramatically according to frame type or story number in all scaling approaches and cases.

In addition to evaluation of the spectral shape compliance, the effect of the scaling approaches and limits on the GM parameters, in other words, intensity measures (IMs) were investigated. Bradley [24] stated that in addition to spectral compatibility of target spectrum, specific IMs of site of interest should also be considered during record selection and suggested a GCIM method to perform record selection. Considering both issues, some salient IMs such as *PGV*, *AI*, *SD* time interval between 5 and 95% of *AI*, *CAV* and *HI* also called spectrum intensity (*SI*) which represent major characteristics of earthquake records, were considered. Furthermore, it has been shown in several studies that some of these IMs are highly correlated or closely related to damage to buildings or infrastructures [34–36]. The considered IMs were calculated for all record scaling approaches and mean of IMs were compared in Fig. 10 for each frame.

Fig. 10 clearly emphasizes that different IM values can be obtained even for the same record scaling approach. This is an expected situation since the record scaling limits and approaches do not consider matching IMs to specific distributions during the selection process. Differences between the approaches are more apparently seen in *SD*, *CAV* and *AI* parameters. If the distribution of *SD* and *CAV* values is carefully inspected, it is possible to state that *SD* and *CAV* values are increasing from A2 to A5 and B1 to B5, respectively. Furthermore, almost identical values were obtained between the frames despite the overall differences in each scaling approach. It can also be accepted that distribution of *PGV* and *HI* parameters slightly close between the record scaling approaches, schemes and even for different frames. Further evaluations will be also made in discussion section considering CDF of some important IMs using GCIM and will be compared to assess effect of scaling approaches.

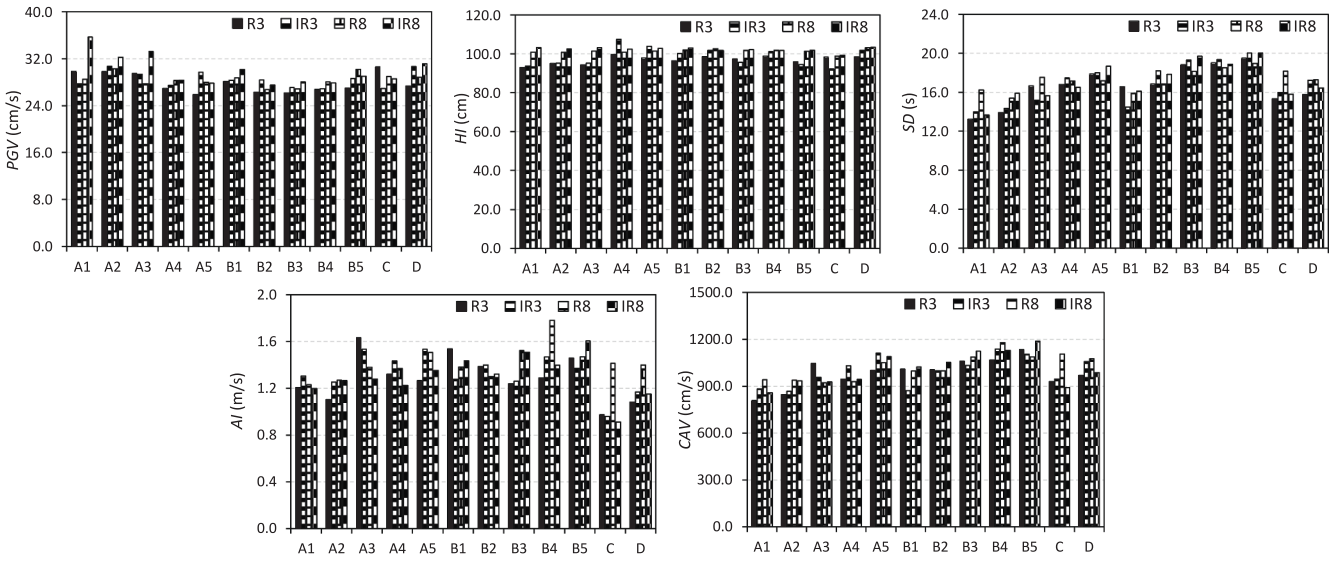

Fig. 10. Distribution of IM values for all frames and approaches.

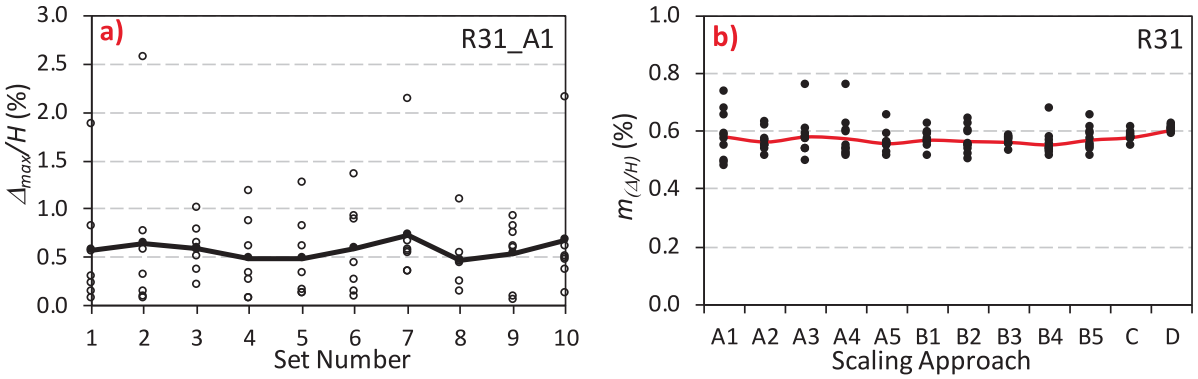

Fig. 11. Determination of seismic responses for scaling approaches considering a sample building (R31).

5. Evaluation of analysis results

In this section, important EDPs determined from each record scaling approach were evaluated in terms of mean and variation of the EDPs for all frames. In this way, the effect of scaling limits and approaches on the EDPs was compared and examined. For this purpose, global (i.e., roof) displacement ratio (Δ/H), inter-story drift ratio (δ/h), and maximum floor acceleration (*MFA*), was used. H and h describe the frame and story height, respectively.

To ease the understanding of notations and give clear perspective about the assessment of seismic demand values given in the manuscript, detailed information and graphical representation of calculations are given for sample frame (R31) and record scaling approach A1 in Fig. 11. As defined in Eurocode-8, each GM record set has seven GM records, and ten GM record sets were used for each selection approach and frame pair considered in this study. Based on an earlier description, one can observe the seven maximum demands of individual GMs (Δ_{max}/H) for each record sets and these values are plotted as black hallow circle in Fig. 11a. Mean of the demands for each record set is also plotted as black filled circles in the same figure and notated as "m" throughout the manuscript. Accordingly, ten $m_{(\Delta/H)}$ values are calculated for A1 approach. If the same procedure is applied to all record selection

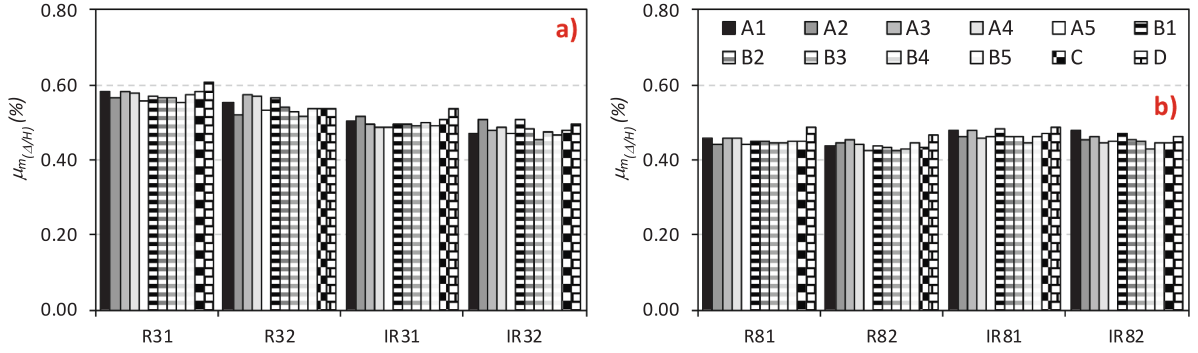

Fig. 12. Comparison of $\mu_{m(\Delta/H)}$ values obtained for scaling approaches (a: three story, b: eight story).

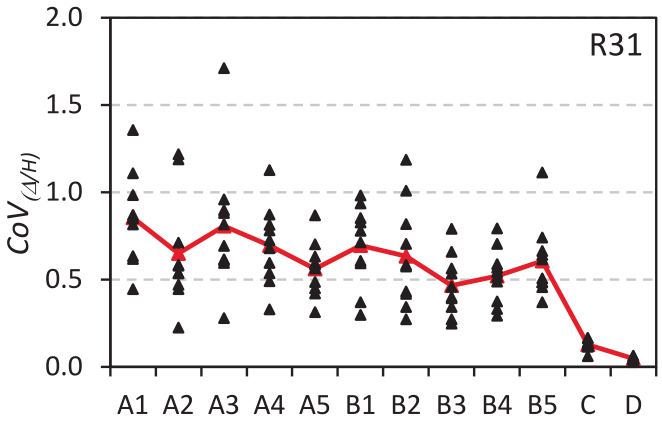

Fig. 13. Dispersion of Δ/H demands versus each scaling approach for R31.

approaches, results can be illustrated as in Fig. 11b. In the figure, ten black filled circles for each approach (e.g., A1) describe $m_{(\Delta/H)}$ values. If the mean of ten $m_{(\Delta/H)}$ values obtained for an approach is calculated (e.g., A1), $\mu_{m(\Delta/H)}$ value (actually the mean of 70 Δ_{max}/H values) is obtained. For roof displacement ratios, $\mu_{m(\Delta\ /H)}$ values are shown as red filled circles in Fig. 11b for each approach.

Distribution of red filled circles for R31 frame is also plotted in Fig. 12 and the values shown in Fig. 11b can also be observed from this figure. The whole procedure made for R31 is also repeated for all the frames and distribution of $\mu_{m(\Delta\ /H)}$ values are illustrated in Fig. 12 for three and eight-story frames, separately. As can be seen, $\mu_{m(\Delta\ /H)}$ values are very close to each other despite the significant differences between the record scaling approaches. $\mu_{m(\Delta\ /H)}$ values are between 0.4 and 0.6. Since the roof displacement demands (Δ) are divided to frame height (H), $\mu_{m(\Delta\ /H)}$ values are decreasing with increasing frame height. Thus, $\mu_{m(\Delta\ /H)}$ value for three-story frames are slightly higher than those for eight-story frames. It can easily be concluded that different scaling limits and approaches have no important contribution on roof displacement ratios if mean responses are considered. Calculations have shown that the variation of $\mu_{m(\Delta\ /H)}$ values given in Fig. 12 is less than 5% between the distinct scaling approaches.

To assess the dispersion of seismic demands considering the record scaling approaches and schemes, coefficient of variation value of global displacement ratio, $CoV_{(\Delta\ /H)}$, was calculated for each record set. $CoV_{(\Delta\ /H)}$ values of GM record sets are plotted in Fig. 13 for R31 building frame as example. Mean of $CoV_{(\Delta\ /H)}$ values for each scaling approach, $\mu_{CoV(\Delta\ /H)}$, is also marked as red filled triangle in the figure. It can be observed from the figure that dispersion of A and B approaches is generally high and dispersion between the distinct record sets is also high. $CoV_{(\Delta\ /H)}$ values determined for C and D approaches, on the other hand, are considerably lower than those for A and B approaches. Furthermore, dispersion of distinct record sets for C and D approaches is also lower than for other approaches. When C and D approaches are compared, it can be said that lower dispersion of seismic demands is obtained for D

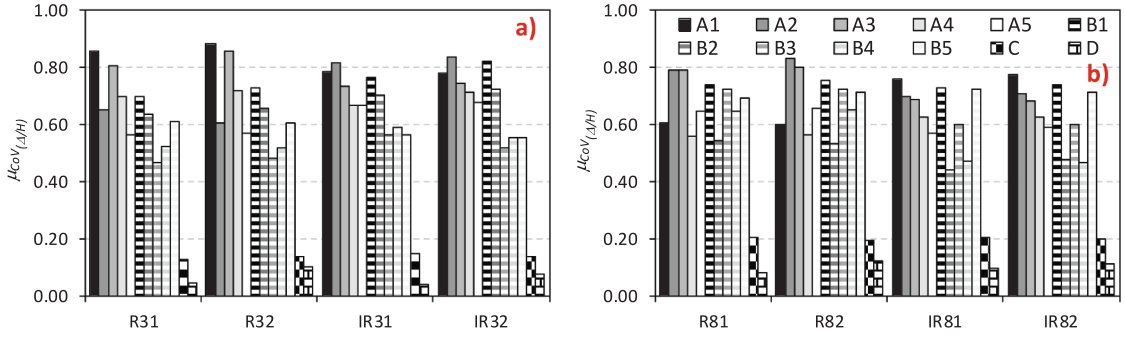

Fig. 14. Dispersion of Δ/H demands for scaling approaches (a: three-story; b: eight-story frames).

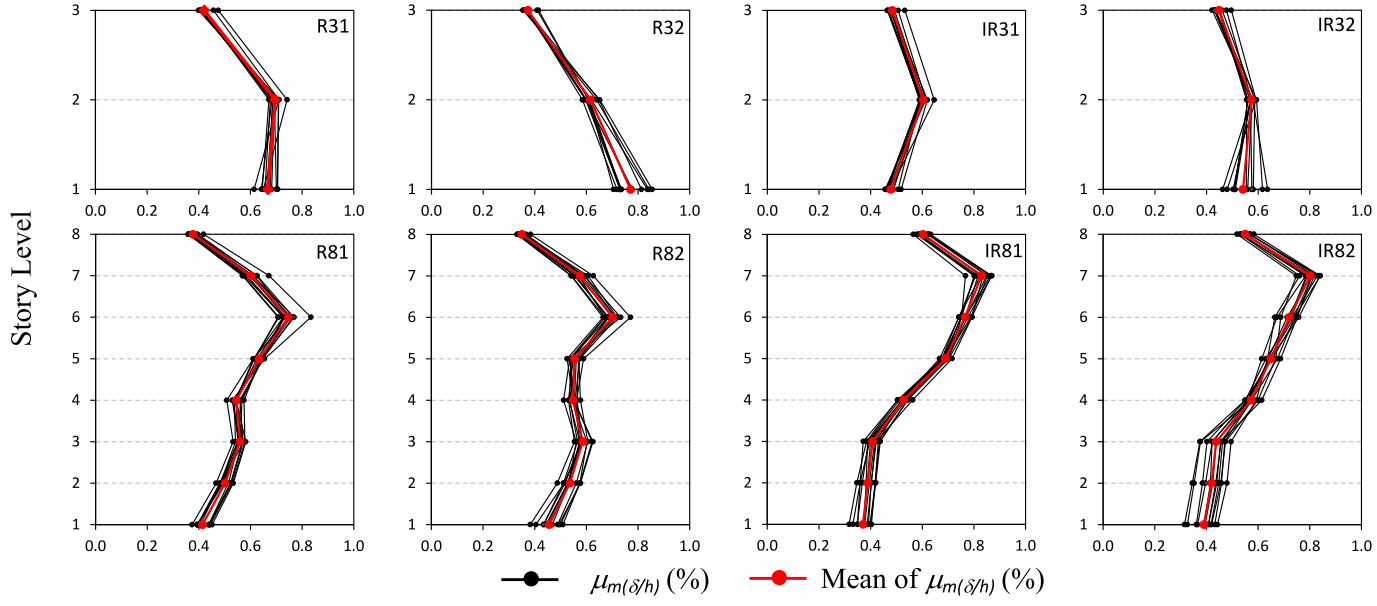

Fig. 15. Distribution of $\mu_{m(\delta\ /h)}$ values along the frame height for all frames and scaling approaches.

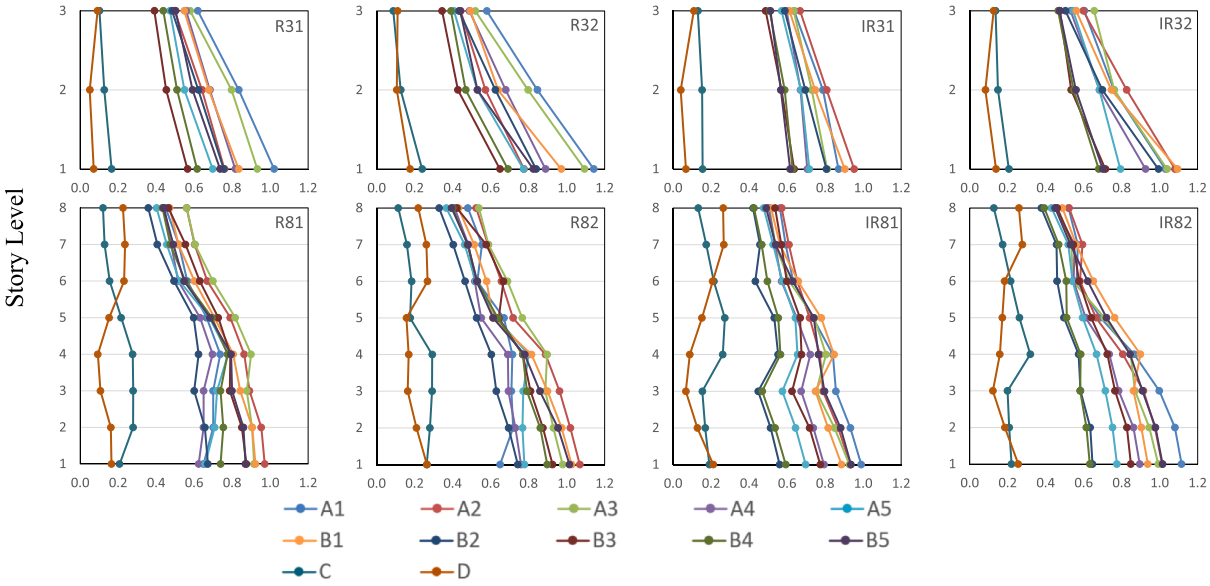

Fig. 16. Distribution of $\mu_{CoV(\delta\ /h)}$ values along the frame height all frames and scaling approaches.

approach. It is worth noting at this point that all record selection schemes have identical strategies to match the same target spectrum, but they may produce very different seismic demands. Various studies have also demonstrated that consideration of spectral compatibility of individual and mean spectra with target spectrum in the selection has important contribution to control the dispersion of seismic demands, supporting this finding [29,30,37].

$\mu_{CoV(\Delta\ /H)}$ values of all frames used in this study according to selection scenarios and scaling approaches are provided in Fig. 14. According to Fig. 14, $\mu_{CoV(\Delta\ /H)}$ values obtained for A and B approaches are generally higher than 0.5 for all the frames and topologies. However, it is hard to give solid evidence about the trend of any case for A and B approaches and it can be admitted that the dispersion of seismic demands is random for these approaches. Observations on the trend of $\mu_{CoV(\Delta\ /H)}$ values implies that the dispersion of seismic demands for C and D approaches have significantly lower than A and B approaches. In addition, D approach has lower dispersion than C approach. $\mu_{CoV(\Delta\ /H)}$ are lower than 0.17 and 0.09 for C and D approaches, respectively. This situation once again exposes the effect of a relationship between spectral shape compliance of individual spectra and target spectrum.

Following the evaluations of the global displacement ratios, the inter-story drift ratio demands, the other important EDP, for each scaling approach were evaluated. In Fig. 15, $\mu_{m(\delta\ /h)}$ values determined for each scaling approach is plotted along the frame height. In the figure, each black dotted line describes the different scaling approaches (e.g., A1, B1, C, etc.) and there are 12 dotted lines for each building frame. Mean of $\mu_{m(\delta\ /h)}$ values obtained for the scaling approaches is also plotted as red dotted line. According to Fig. 15, $\mu_{m(\delta\ /h)}$ values determined for scaling approaches are mainly range around 0.3–0.9% for both frames regardless of frame irregularity. Depending on the mass and stiffness distribution in the story levels, inter-story drift ratio demands are increasing in irregular frames at upper stories compared to regular frames. For example, mean of $\mu_{m(\delta\ /h)}$ values for R82 are 0.46%, 0.54%, 0.59%, 0.55%, 0.55%, 0.70%, 0.57% and 0.35% while mean of $\mu_{m(\delta\ /h)}$ values for IR82 are 0.39%, 0.42%, 0.44%, 0.57%, 0.65%, 0.72%, 0.80%, 0.55% from 1st to 8th story, respectively. In fact, it is natural to obtain different drift ratios according to different scaling approaches, although they consider compatibility with the same target spectrum. Nevertheless, it

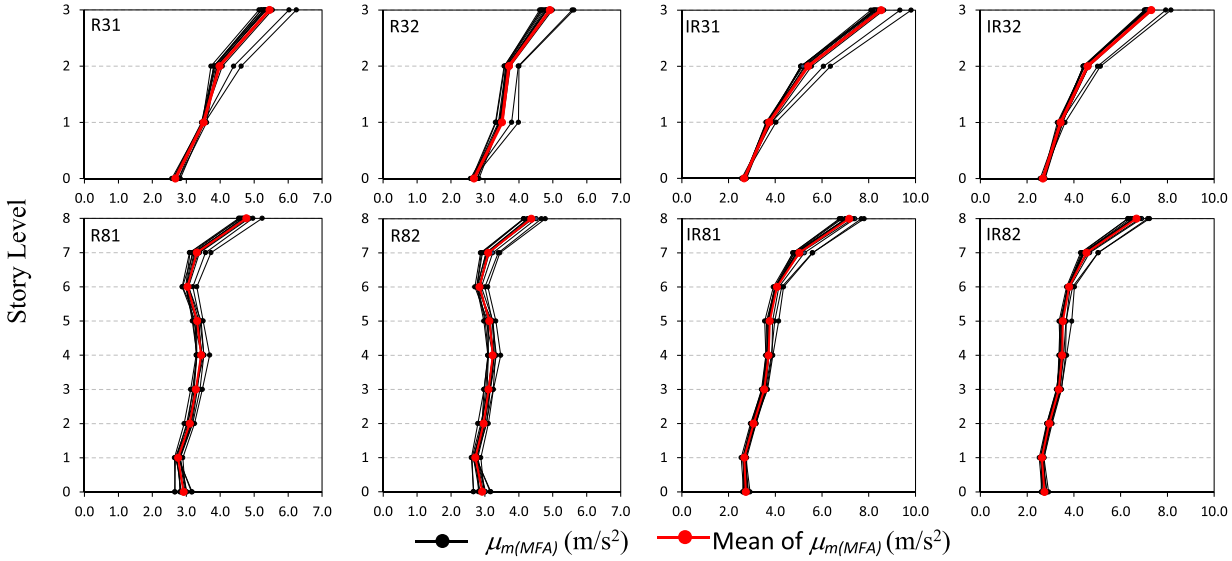

Fig. 17. Distribution of $\mu_{m(MFA)}$ values along the frame height all frames and scaling approaches.

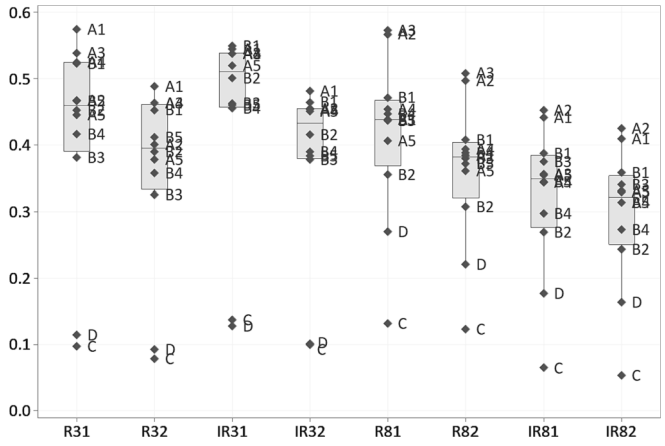

Fig. 18. $\mu_{CoV(MFA)}$ of all building frames at the roof story considering all scaling approaches.

can be said that $\mu_{m(\delta\ /h)}$ values produced from different approaches seem close to each other.

Consideration of mean seismic responses is adequate to make seismic design or assessment according to seismic codes and distribution of $\mu_{m(\delta\ /h)}$ values obtained for various scaling approaches seems very close. Accordingly, obtained results from different scaling approaches seem convincing for seismic codes despite the small differences which are assumed to be due to the random nature of record selection. However, mean seismic responses may not be sufficient for probabilistic methods and these methods also concern the variation of seismic responses since the variation can be used to explain the dispersion and sensitivity of the event. For this reason, $\mu_{CoV(\delta\ /h)}$ values were also calculated for scaling approaches and frames and illustrated in Fig. 16. It can be observed from the figure that $\mu_{CoV(\delta\ /h)}$ values for A and B approaches are usually high, and it can be admitted that these values are not correlated with scaling approach. In other words, it cannot be said that a specific scaling approach has a significant effect on the dispersion of seismic demands obtained for the frames. For example, A1 approach provides the highest dispersion in frames R31 and R32, but this situation is not observed for the other frames. Similar conclusion can also be made for other scaling approaches. $\mu_{CoV(\delta\ /h)}$ values for A and B approaches are higher at first stories and the dispersion tend to decrease at upper stories.

According to Fig. 16, it can be concluded that A&B and C&D approaches are clearly separated, and the dispersion of seismic demands for C&D approaches is significantly lower. This situation once again indicates that considering the compatibility of individual spectra of GM records with target spectrum apparently affects the dispersion more than the mean. In general, it can be said that dispersion of seismic demands for D approach is slightly lower than those for C approach and the demands tend to converge to each other at higher stories. $\mu_{CoV(\delta\ /h)}$ values for these scaling approaches crossover at 5th and 6th stories in eight-story building frames. $\mu_{CoV(\delta\ /h)}$ values for A and B approaches are around 0.60 while they are around 0.20 for C and D approaches.

The last EDP used for evaluation is maximum floor acceleration demand (*MFA*). The distribution of $\mu_{m(MFA)}$ values calculated for each scaling approach is plotted in Fig. 17 as black dotted lines for all frames. In the figure, a red dotted line describes the mean of $\mu_{m(MFA)}$ values calculated for all scaling approaches from A1 to D. Fig. 17 indicates that *MFA*s are prone to increase from base to roof story and the highest *MFA*s are observed at roof story. $\mu_{m(MFA)}$ values of irregular frames are considerably higher than regular frames at roof level. Fig. 17 also shows that $\mu_{m(MFA)}$ distribution of different approaches is closely related compared to distribution of $\mu_{m(MFA)}$. Observations showed that the highest *MFA*s were obtained for C and D approaches, and this is valid regardless of regularity of the frames. The difference in $\mu_{m(MFA)}$ values

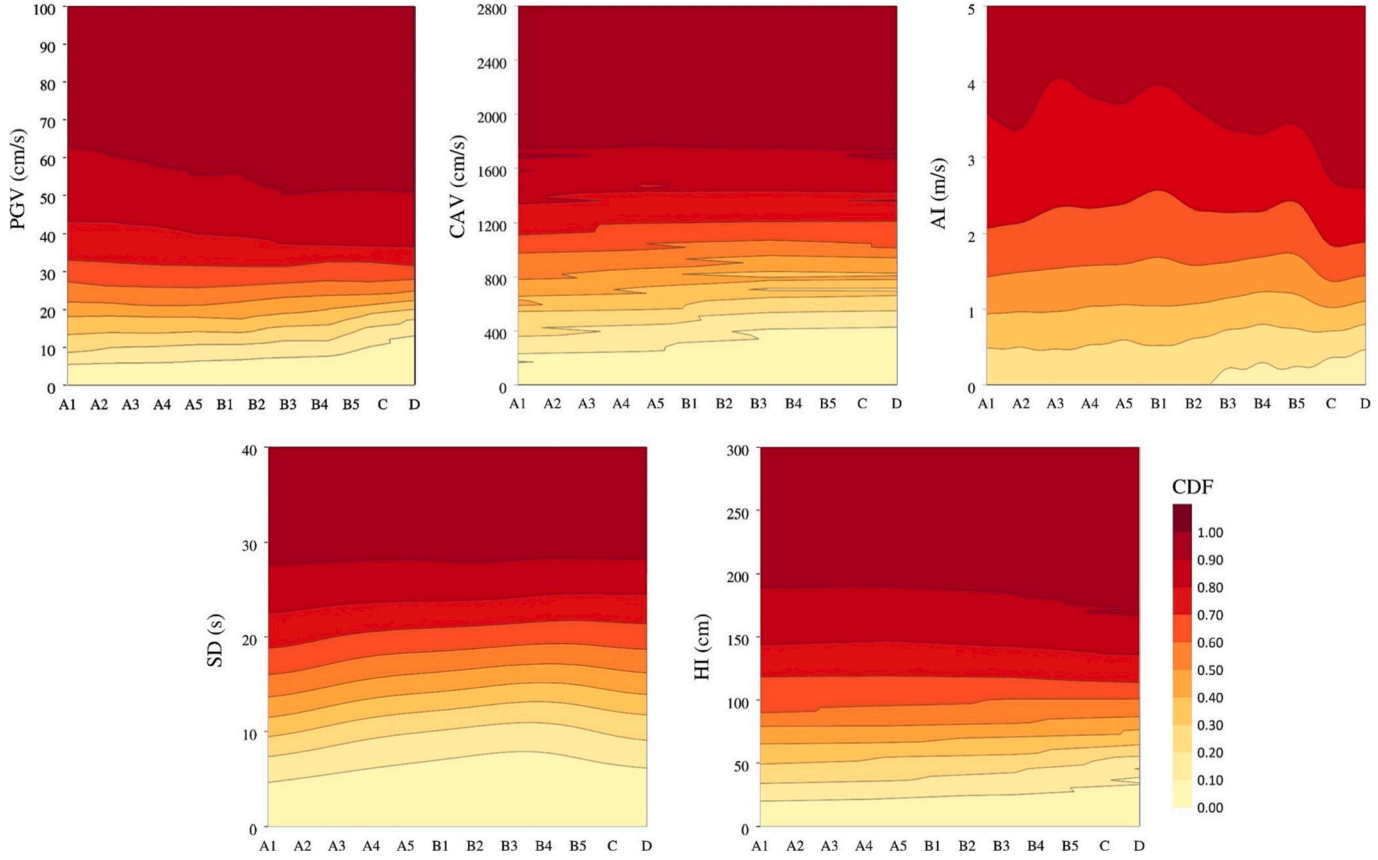

Fig. 19. Contour map of cumulative probabilities of *PGV*, *CAV*, *AI*, *SD* and *HI* for R3 frame.

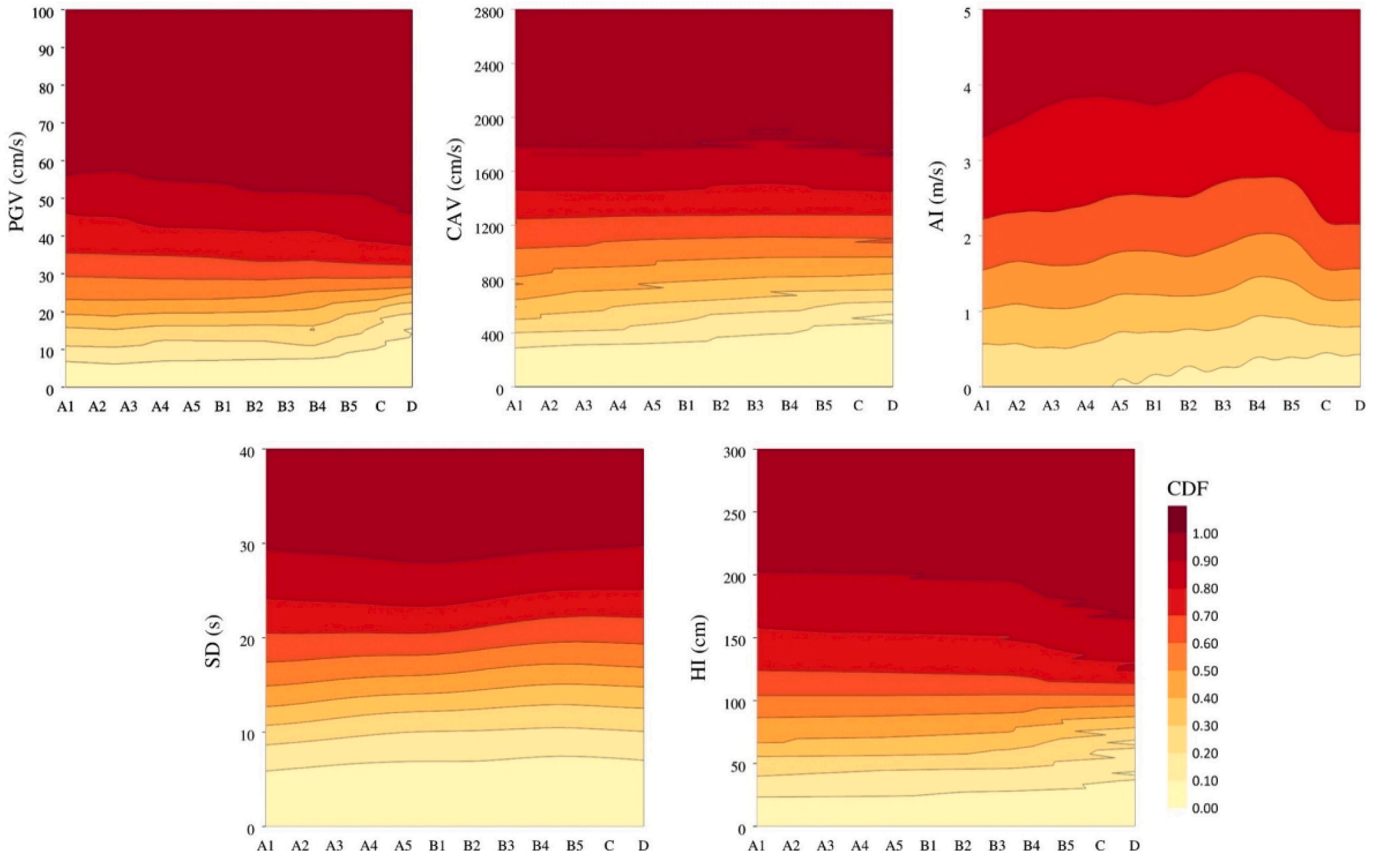

Fig. 20. Contour map of cumulative probabilities of *PGV*, *CAV*, *AI*, *SD* and *HI* for R8 frame.

between the C&D and other approaches can be seen especially at the roof story. Authors think that this situation is occurred due to spectral shape compatibility of individual records with target spectrum. Spectral shape comparison of scaling approaches was shown earlier in Fig. 5. If the spectral shape of individual records of C&D approaches are compared with A&B approaches, it can be realized that spectral compatibility of individual records for C&D approaches are generally higher between 0.2 *T* and 2.0 *T* range or at natural period of building (*T**). On the other hand, spectral accelerations of the records selected using A&B approaches may be higher or lower than the target spectral acceleration between the predefined period range or building specific period. Therefore, *MFA* values of C&D approaches are relatively higher than A&B approaches.

To evaluate dispersion of *MFA* values, $\mu_{CoV(MFA)}$ values for all scaling approaches were calculated just for last story of frames since the highest *MFA*s were observed at this this story. Individual values of approaches such as median, first and third quartiles of $\mu_{CoV(MFA)}$ values are provided via boxplot in Fig. 18. It can be seen from the figure that C&D approaches have the lowest variation, and the dispersion of *MFA*s for C approach is generally lower than D approach especially for eight-story frames. It can be also observed that C approach is always outliers for three and eight-story frames regardless of irregularity while D approach is not for eight-story frames. This situation implies that these methods diverge from other approaches in terms of $\mu_{CoV(MFA)}$ values. $\mu_{CoV(MFA)}$ of C and D approach is around 0.1 and 0.16 in average, respectively. Fig. 18 expresses that A1, A2, A3 and B1 approaches are generally higher than 1st quartile which means that they relatively have higher variation compared to A4, A5 and rest of B approaches.

6. Discussions

Following the evaluations on the analysis results considering commonly used EDPs, CDF of some IMs were evaluated to understand whether different record scaling schemes and approaches influenced the distribution of IMs. In addition to evaluations on the distribution functions of IMs, non-exceedance probability curves of EDPs were obtained for all selection scenarios and scaling approaches considering all structural topologies. By this way, the effect of scaling limits and approaches on the probabilities of EDPs were investigated and compared.

In this study, CDF of IMs were evaluated by two cases. In the first case, just CDF of IMs given in Section 4 were calculated and compared. This case will purely enable to compare and observe at a time how scaling approaches affect the IMs for different structural topologies. In Figs. 19 and 20, contour maps of cumulative probabilities of *PGV*, *CAV*, *AI*, *SD* and *HI* are plotted for R3 and R8 building frames considering all selection scenarios and scaling approaches. When the contour map of R3 building is investigated, a gradual increase can be observed especially for *PGV*, *HI* and *SD*. Despite the slight fluctuations between some scaling approaches at high *AI* values, gradual change can also be seen for *AI*. Cumulative probability maps for C and D approaches are lower at low *PGV* and *HI* levels, but high probabilities can be observed at high *PGV* and *HI* levels for these approaches. This situation means that C and D approaches have steeper cumulative probability curves than other approaches. Similar trend can also be observed for B3, B4 and B5 approaches in addition to C and D approaches for *CAV* and *AI*. When the CDF of *CAV* is checked, sawtooth shape like formations can be observed at some *CAV* levels between the different scaling approaches. This situation simply reveals the transition of cumulative probabilities between the different scaling approaches at some levels of *CAV*. Nevertheless, it can be admitted that especially cumulative probability for C and D approaches is steeper than others. This situation might be due to consideration of individual spectra in the record selection process. Compared to others, *SD* has smoother cumulative probability curves, and they gradually increase at different *SD* levels for all scaling approaches. It can

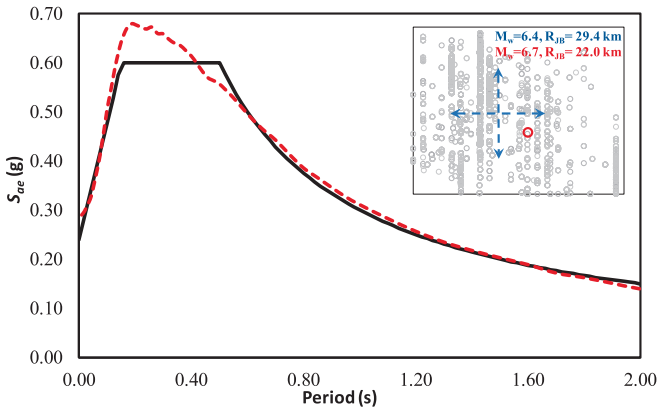

Fig. 21. Comparison of design and scenario-earthquake hazard spectrum.

be apparently claimed that cumulative damage probabilities of scaling approaches are almost linear which means that all approaches have almost the identical shape and they are almost parallel to each other. Contour map of R8 frame is also illustrated in Fig. 20 for comparison with R3 frame and it can be said that similar conclusion can also be drawn for R8 building frame. CDF of same IMs were also calculated for IR3 and IR8 and evaluations on the cumulative probabilities have shown that trend of curves almost similar to their counterparts of R3 and R8, respectively.

In the second case of evaluations, CDF of some IMs were compared with target CDF of corresponding IMs using GCIM method proposed by Bradley [24]. By this way, the relationship between the calculated CDF and target cumulative probabilities was investigated. It is worth noting that GM records used for the analysis of frames might not comply with target CDF since they are not selected considering the GCIM method. However, target CDFs were considered as reference to understand the tendency (e.g., location, gap, transition etc.) of scaling approaches with target ones using cumulative probability curves. According to GCIM, specific IMs concerning the construction site for the interest of structural analysis should be determined. Accordingly, target CDF of selected IMs can be determined via deterministic or probabilistic seismic hazard analysis (SHA) results. In this study, target IMs were selected as *PGV*, *SD* and *AI* considering their importance and close relation on the damage potential of structures and parameters of regarding IMs was computed from GMPEs developed for *PGV*, *SD* and *AI* [38–40]. For this purpose, moment magnitude (M_w) and Joyner-Boore distance (R_{JB}) of selected GM records were used to determine the target CDFs utilizing the deterministic SHA approach. Potential earthquake pairs (M_w and R_{JB}) were obtained by compiling the hazard spectrum of scenario-earthquake determined from ground motion prediction equation (GMPE) and spectral shape of uniform hazard spectrum used for the design of frames also considering design soil class. GMPE proposed by Akkar et al. [41]

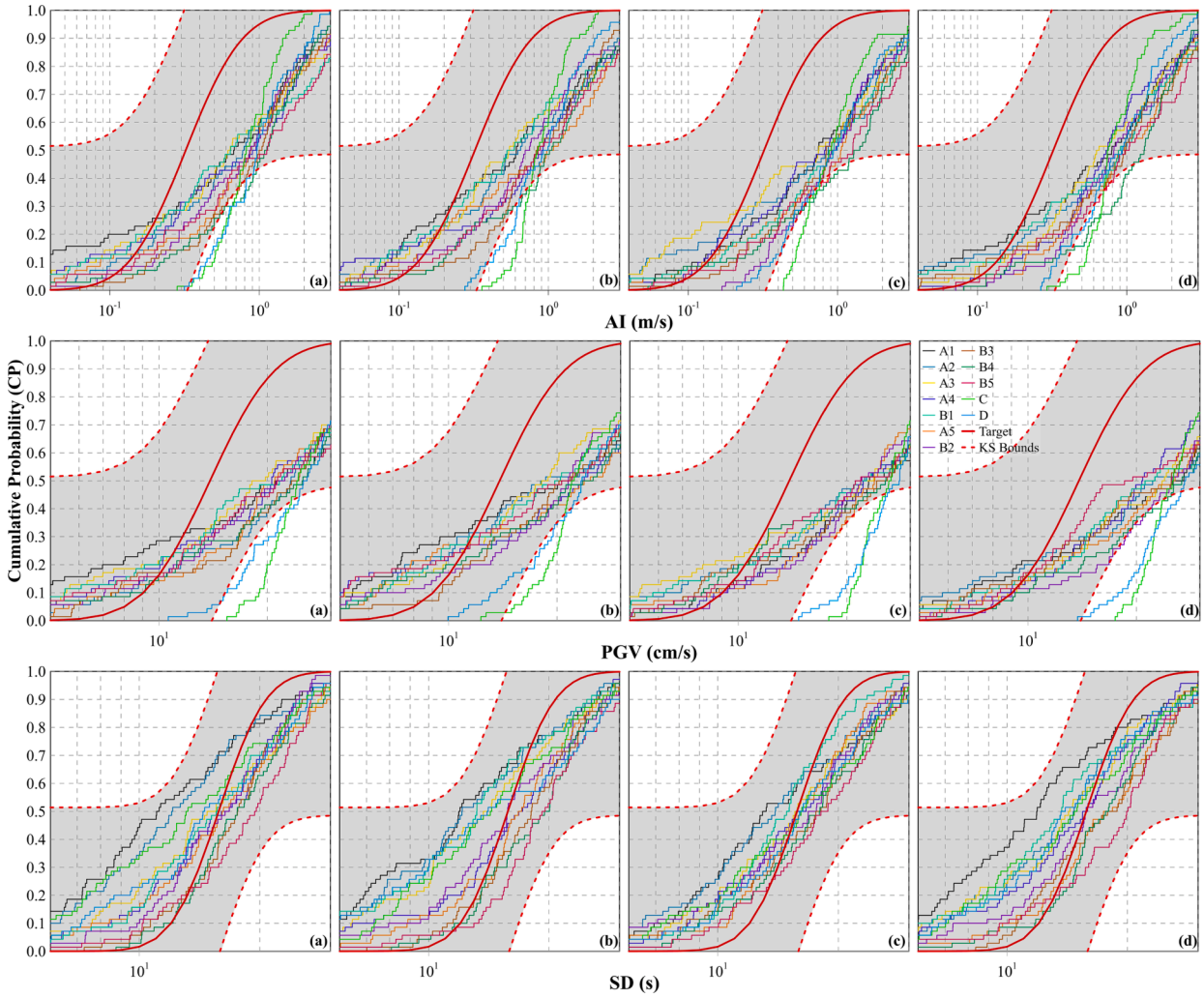

Fig. 22. Comparison of cumulative probabilities of different scaling approaches with target and KS bounds for all frames (**a**. R3, **b**. IR3, **c**. R8, **d**. IR8) using deterministic earthquake scenario ($M_w = 7.6$, $R_{JB} = 22$ km).

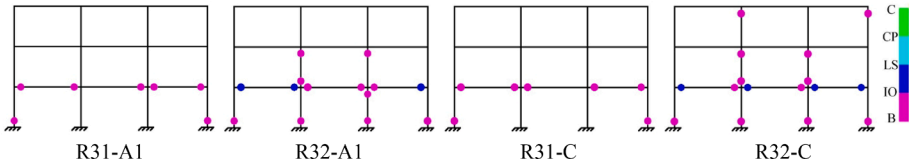

Fig. 23. Plastic formation of three-story regular buildings for A1 and C approaches.

was used to compute the hazard spectrum of scenario-earthquake. Consequently, the target scenario-earthquake was determined as $M_w = 6.7$, $R_{JB} = 22$ km and $V_{s30} = 380$ m/s for $\varepsilon = 1.0$. A comparison of target and computed spectrum for soil B is plotted in Fig. 21. It can be seen from the figure that the scenario-earthquake has good agreement with target spectral acceleration spectrum used for the design of considered frames. In the figure, spatial distribution of GM records used for the analysis of frames represented by grey hollow circles with their mean ± std. deviation (blue dashed lines) of M_w and R_{JB} and scenario-earthquake represented by red hollow circle, can be compared.

Following the determination of scenario-earthquake, target CDF of selected IMs and their 5% confidence interval (bounds) using Kolmogorov Smirnov (KS) test were computed to include probabilistic approach. Computed target cumulative probabilities and KS bounds for *PGV*, *AI* and *SD* are illustrated with cumulative probabilities of selection scenarios and scaling approaches for all frames in Fig. 22. Cumulative probabilities of scaling approaches for *AI* were almost identical except C and D for all frame types and it is apparent that C and D approaches were out of the KS bounds at some levels of *AI*. It can be said that the arm of the *AI* becomes steeper for A and B approaches with increasing *AI*. Systematic order is not observed between the curves or frame topologies. It is possible to suggest that C and D approaches follow almost similar trajectory with target CDF, but also resembles the postponed state of the target. Although GMs are not selected considering the target CDF of *AI*, majority of the curves satisfy the IM conditioned selection, and it seems that minor improvement can be made to fully satisfy all conditions.

Similar to *AI*, cumulative probabilities of A and B approaches for *PGV* are mostly between the KS bounds for all frame types and an important portion of C and D approaches are out of the KS bounds for especially 8-story frames. Very limited part of B2 and B4 approaches are out of KS bounds especially for IR8 building frame. Systematic arrangement cannot be done between the curves or frame topologies, but probability curve tendency of A and B approaches are likely linear, and they tend to separate from the target curve with increasing *PGV*. C and D approaches still resemble the target ones, but *PGV* of these approaches at low probabilities are higher when compared to target probabilities. Compared to *AI* and *PGV*, cumulative probability curves of all approaches for conditioning *SD* are between the KS bounds of target CDF. All approaches have similar pattern and probabilities are gradually increasing with increasing *SD*. Similar conclusions were also made earlier, as shown in Figs. 19 and 20. Although there is no still systematic order between the approaches, A1 and B5 are likely the upper and lower limits for all scaling approaches since other approaches are consistently between them for all frame types. Overall evaluation of cumulative probability distributions has illustrated that neither scaling limits nor scaling approaches have apparent influence on cumulative probabilities. Furthermore, systemic relation between the scaling limits or approaches in terms of probabilities is not noted.

In evaluation of analysis results, building responses such as global (or roof) or inter-story displacements demands were presented. It can be claimed that these structural demand parameters are important for the design and assessment if analyst applies the displacement-based procedure. In performance-based perspective, analyst should also control the seismic displacement demand from the target spectrum and should compare the capacity with the demand to decide the performance of building. Furthermore, in current design practices of seismic codes [1–3] such as force-based design, displacement demands especially inter-story drift ratios are controlled for ductile design, determination of vertical and horizontal irregularities for buildings and to avoid excessive displacement differences between the upper or lower stories. However, plastic hinge formation of buildings can be also important to make decision about the building such as strengthening or demolish. Therefore, analyst should check the damage mechanism and performance state of each element. Considering this issue, plastic hinge formation of buildings including damage states at the plastic hinges are compared for different scaling approaches and scaling limits.

It should be noted that there are five cases for approaches A and B and totally, there are 12 scaling approaches applied to each building. To avoid repetition of figures and to represent the comparison of unscaled and scaled ground motion records, only plastic formation A1 and C approaches was compared. Mean rotation demands were calculated and compared with deformation capacities to determine damage state of each member. In Figs. 23 and 26, plastic hinge formation of buildings is plotted. Plastic hinge distributions indicated that buildings designed only by gravity loads (i.e., R32, IR32, R82, IR82) were experienced higher damages compared to seismically designed buildings (i.e., R31, IR31, R81, IR81). It was observed that plastic rotation demand of eight-story buildings was higher than three-story buildings especially in first story of buildings. Plastic deformation demands were generally reduced at upper stories resulted in less plastic hinges for both group of buildings. When the plastic hinge distribution of regular buildings (see Figs. 23 and

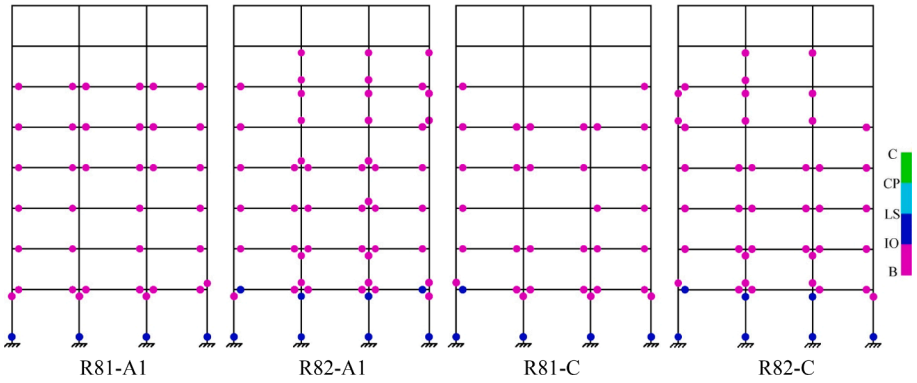

Fig. 24. Plastic formation of eight-story regular buildings for A1 and C approaches.

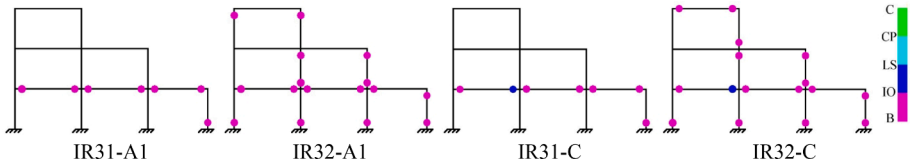

Fig. 25. Plastic formation of three-story irregular buildings for A1 and C approaches.

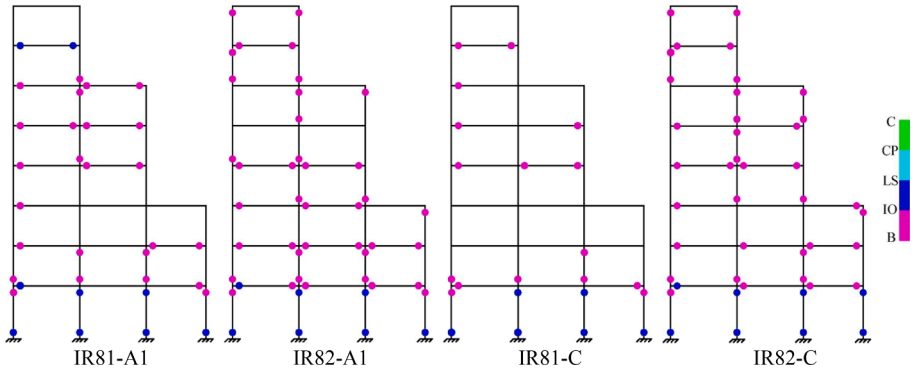

Fig. 26. Plastic formation of eight-story irregular buildings for A1 and C approaches.

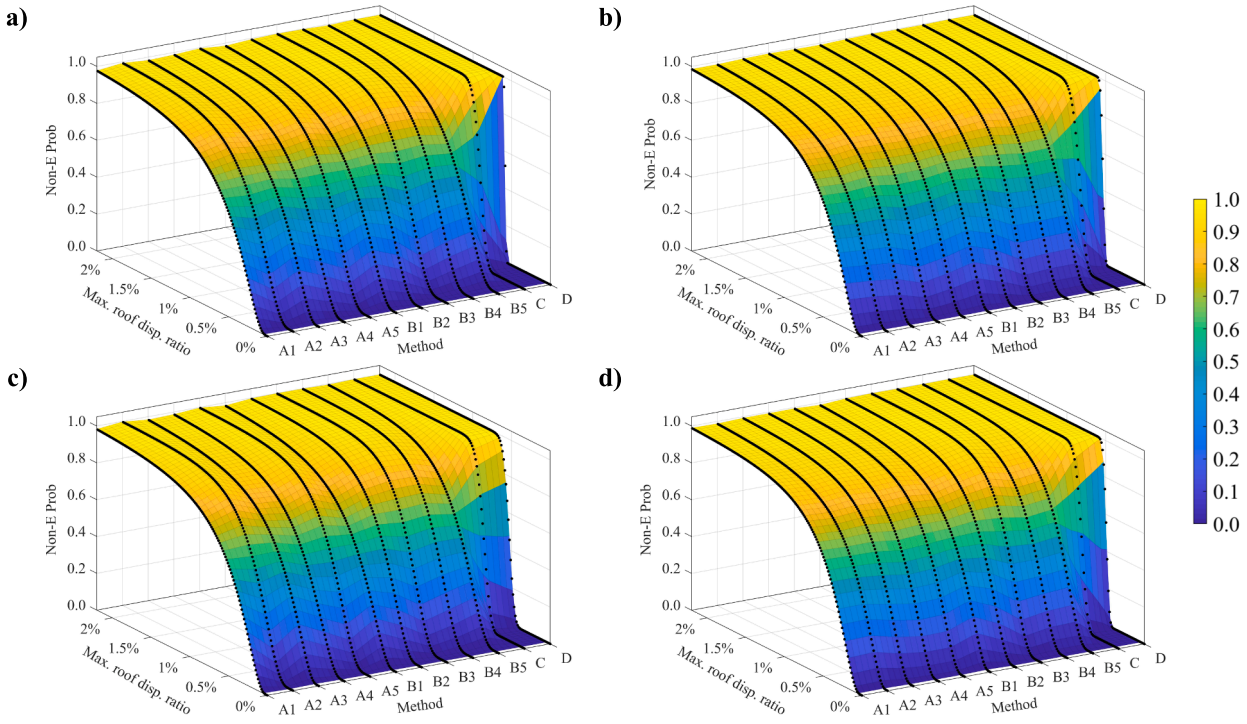

Fig. 27. Non-exceedance probability surfaces of scaling approaches for Δ/H (**a**. R31, **b**. IR31, **c**. R32, **d**. IR32).

24) for different selection and scaling approaches are compared (i.e., A1 and C approaches), it can be said that damage states of members are mostly similar. In addition to similarity of damage levels, damage localization in columns and beams along the building height is analogous. This situation is also valid for irregular building as can be observed in Figs. 25 and 26. Although other scaling approaches were not presented here, plastic hinge formation of building were checked for other approaches. It can be admitted that similar plastic hinge distributions were also observed for C, D and all cases of A and B approaches.

To evaluate the effect of scaling limits and scaling approaches, a probabilistic approach was also considered and non-exceedance probability curves of maximum global (i.e., roof) displacement ratio (Δ/H), inter-story drift ratio (δ/h) and *MFA* demands were investigated. To make a comprehensive assessment for each frame and EDP between the approaches, fragility curves and surfaces were plotted by a color map accounting probabilities at each level of EDPs.

In Fig. 27, non-exceedance probability curves and surfaces of three-story buildings including irregular ones are shown as black dots for each approach considering Δ/H demand. It can be realized from the figure that the probability curves of C and D differ from the A and B approaches. This situation is also valid for regular and irregular frames. Despite the small differences between the regular and irregular frames in

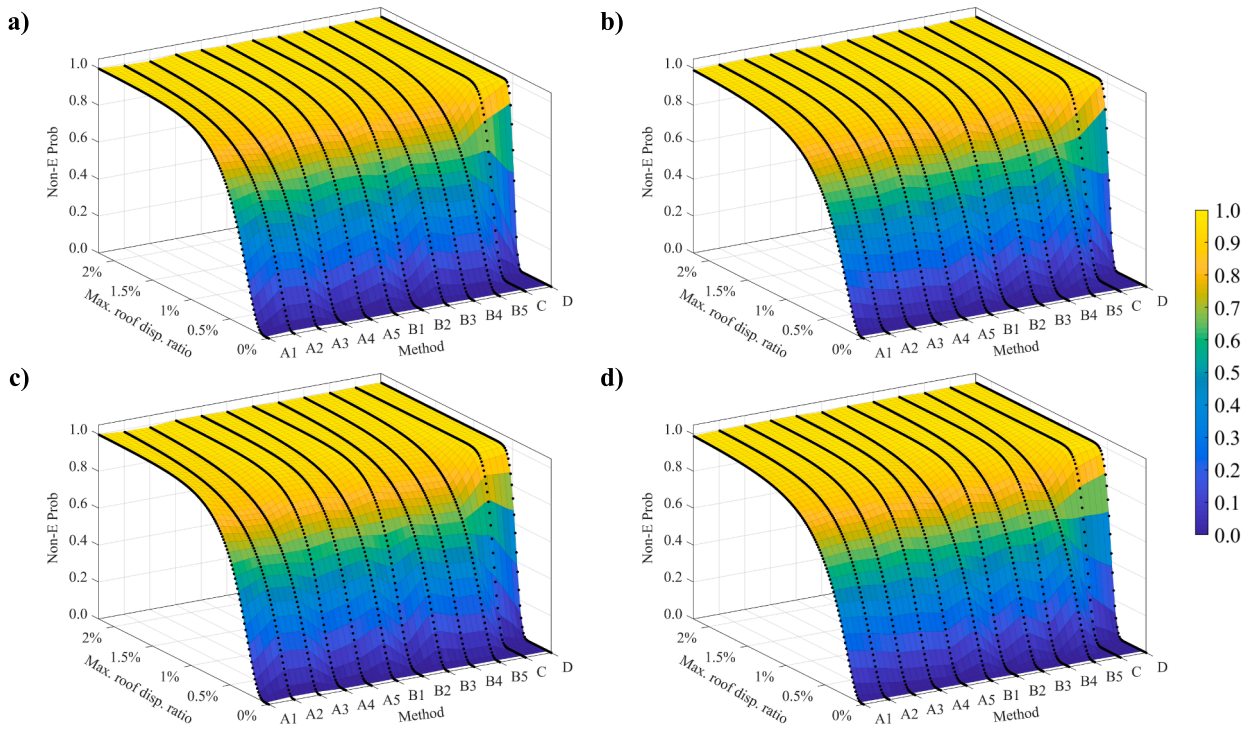

Fig. 28. Non-exceedance probability surfaces of scaling approaches for Δ/H (**a**. R81, **b**. IR81, **c**. R82, **d**. IR82).

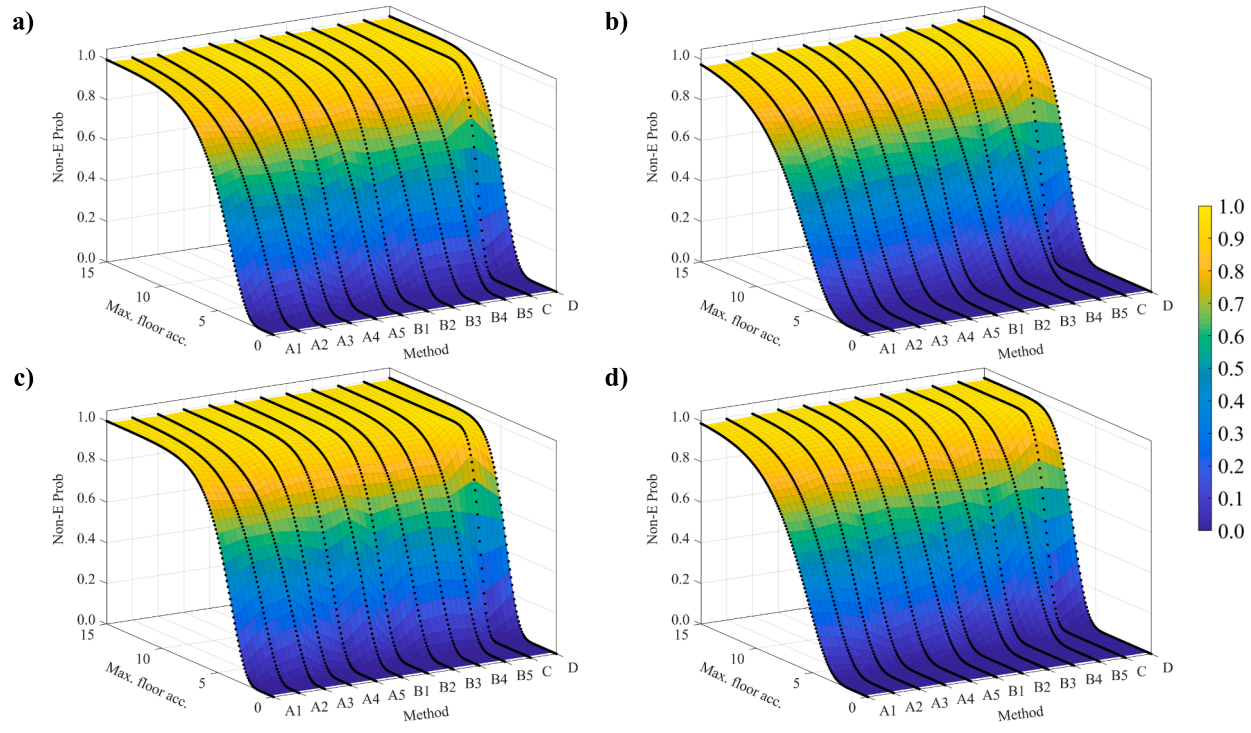

Fig. 29. Non-exceedance probability surfaces of scaling approaches for *MFA* (**a**. R81, **b**. IR81, **c**. R82, **d**. IR82).

terms of probabilities, the probability curves of A and B approaches are almost identical regardless of scaling approach. Apparent divergence is not observed between the approaches and the approaches may intertwine at different level of Δ /H. It was observed that all approaches overlapped at ratio of 0.5% and non-exceedance probability of Δ /H is 0.6. Rapid increases were observed in non-exceedance probability curves of C and D approaches especially around the 0.5% when compared with A and B approaches. In addition, it can be said that probability curves of D approach are steeper than C approach. In fact, this is an expected situation since these approaches have specific constraints for spectral matching of GM records and selected GMs and have less variation of spectral accelerations around the target spectrum. Accordingly, the dispersion of Δ/H demands has less variance, and this situation resulted the rapid increase in probabilities. However, these

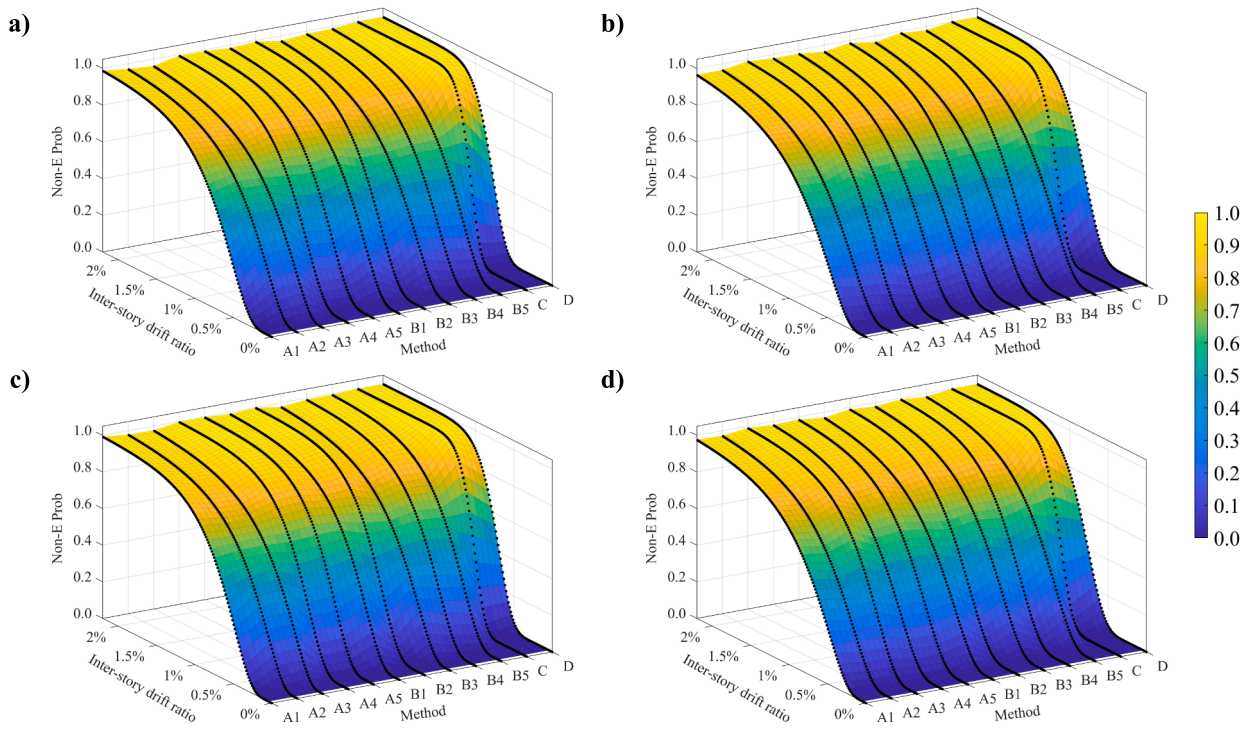

Fig. 30. Non-exceedance probability surfaces of scaling approaches for δ/h (**a**. R81, **b**. IR81, **c**. R82, **d**. IR82).

approaches have not an apparent effect on mean seismic demands as also stated in previous sections. If the comparison of C and D approaches is made, it can be said that D approach has a rapid increase than C in terms of non-exceedance probabilities. It should be noted that D approach is concentrated on selecting records with zero variation in terms of spectral accelerations at a specific period (T^*). Since frame type structures are studied, they can be accepted as first mode dominant structures and this situation explains the rapid increase in probability curves. Non-exceedance probability surfaces of Δ/H demand for eight-story buildings are also illustrated in Fig. 28. Similar to three-story buildings, significant differences in terms of Δ $/H$ demands are not observed between A and B approaches. This situation indicates that scaling approaches have no apparent effect on damage probabilities in eight-story frames as observed in low-rise three-story frames.

In Fig. 29, non-exceedance probability surfaces of *MFA*s at roof story level for eight-story frames are plotted and actual probability curves are shown as black dots in the figure. *MFA*s for three-story buildings are not shown to avoid repetition due to similarities between the non-exceedance probability curves as also observed in Δ $/H$ demands. Units of *MFA*s in the figures are in m/s^2. It can be seen from the figure that A and B approaches have very good agreement between each other in terms of probabilities compared to C and D approaches. Non-exceedance probability curves of approaches intersect at the around 5 m/s^2 (0.51 g) for regular frames and 8 m/s^2 (0.81 g) for irregular frames. Intersection point is described as where the same probability is observed between non-exceedance probability curves (shown as black dotted lines in the figures) of distinct approaches. Investigations revealed that non-exceedance probability curves of *MFA*s between the A and B approaches are more dispersed than other EDPs for analyzed frames. In general, C and D approaches have a more rapid increase in probabilities among all approaches. Comparison of C and D approaches indicates that non-exceedance probabilities of C are generally higher than D at different levels of *MFA* for three-story frames while the intersection point of *MFA* plays a key role in eight-story frames.

Although significant differences are not observed between C and D approaches before or after intersection point of *MFA* for eight-story buildings as seen in Fig. 29, non-exceedance probabilities of C are lower than D before intersection point which is 0.51 g and 0.81 g for regular and irregular frames, respectively. Consequently, overall probability curves derived for *MFA* showed that non-exceedance probabilities were not affected from the scaling approach owing to very similar tendency between A and B approaches and probabilities are not sensitive to extreme scaling values lower or higher than unity. On the other hand, differences were resulting from record selection strategy which considers the spectral compatibility between the target and individual spectrum of selected records.

Non-exceedance probability surfaces of eight-story buildings are plotted with actual probability curves shown as black dots in Fig. 30 for δ $/h$ which is also important parameter for seismic design and performance evaluation of structures. As mentioned in the previous section, maximum δ $/h$ values were observed at sixth for regular and at seventh story for irregular frames. Accordingly, non-exceedance probability curves are calculated and plotted in Fig. 30 for sixth and seventh stories of regular and irregular frames, respectively. The figures clearly indicate that neither regularity of frame nor δ $/h$ levels at different stories influences the non-exceedance probabilities between the A and B approaches. In fact, probabilities are affected by the record selection scenarios and additional constraints to include spectral compatibility of individual GMs with target spectrum dramatically alters tendency of curves.

7. Summary and conclusions

The effect of real GM amplitude scaling for spectrum-compatible record selection according to Eurocode-8 were evaluated with various scaling approaches by adopting different scaling ranges. Simply, four scaling approaches named as A, B, C and D based on the spectral compatibility of mean or individual spectra were used. Real GM record sets were selected using a stochastic solution algorithm for all selection scenarios and scaling approaches, and results were evaluated in two ways. First, maximum global drift ratio, maximum inter-story drift ratio and maximum floor acceleration demands of regular and vertically irregular three and eight story RC frames were evaluated by comparison of distribution of mean and dispersion. Second, non-exceedance

probability curves of the demands and probability distribution of some IMs using GCIM method were compared and assessed. The main findings can be described as follows:

1) Observations showed that amplitude scaling of GMs had no significant influence on the distribution of global drift ratios if only mean responses were considered as recommended by Eurocode-8.
2) Distributions of inter-story drift ratios mainly changed around 0.3–0.9% regardless of building topology. The ratios were increasing in irregular frames at upper stories compared to regular ones. Nevertheless, mean inter-story drift ratios according to different scaling approaches and selection scenarios were compatible.
3) It was observed that spectral accelerations of GM sets obtained from C and D approaches, considering both mean and individual shape compatibility, were slightly higher than A and B approaches which consider only the mean spectrum compatibility. Therefore, *MFA*s of C and D approaches were slightly higher than A and B approaches. Nevertheless, amplitude scaling did not notably influence the mean *MFA*s of A and B approaches.
4) It was noted that dispersion of seismic responses obtained for A and B approaches was considerably higher than that of C and D approaches due to larger spectral ordinate dispersion. It should be also added that dispersion of seismic responses is not dependent on scaling limits.
5) Trend of *PGV*, *AI*, *SD, CAV* and *HI* distributions for the approaches was almost similar. Neither systematic order nor clear building type or topology effect were observed.
6) According to GCIM method results, CDF of A and B approaches for conditioning *PGV*, *AI* and *SD* were between KS bounds of target CDF in general. However, C and D approaches satisfied only SD conditioned selection. Nevertheless, it should be reminded that GMs in the record sets were not selected using GCIM.
7) Non-exceedance probability curves of maximum global (i.e., roof) displacement ratio, inter-story drift ratio and *MFA* apparently indicated that neither building regularity nor amplitude scaling significantly influenced the probabilities between the A and B approaches. In fact, it was monitored that additional constraints including spectral compatibility of individual GMs with target spectrum dramatically altered tendency of curves.

Declaration of Competing Interest

The authors declare that they have no known competing financial interests or personal relationships that could have appeared to influence the work reported in this paper.

References

[1] CEN. ENV 1998–1 Eurocode 8: Design of structures for earthquake resistance—Part 1: General rules, seismic actions and rules for buildings. Brussels, Belgium: European Committee for Standardization; 2004.
[2] ASCE. Minimum design loads and associated criteria for buildings and other structures (ASCE/SEI 7–16). Reston, Virginia, USA: American Society of Civil Engineers; 2017.
[3] TBEC. Turkish building earthquake code. Türkiye: TC Resmi Gazete Ankara; 2018. p. 30364.
[4] Ambraseys NN, Douglas J, Sigbjörnsson R, Berge-Thierry C, Suhadolc P, Costa G, et al. Dissemination of European strong-motion data, VOLUME 2. 13th World Conference on Earthquake Engineering, Vancouver, Canada: 2004, p. 1–12.
[5] Akkar S, Sandıkkaya MA, Şenyurt M, Azari Sisi A, Ay BÖ, Traversa P, et al. Reference database for seismic ground-motion in Europe (RESORCE). Bull Earthq Eng 2014;12:311–39. https://doi.org/10.1007/s10518-013-9506-8.
[6] Ancheta TD, Darragh RB, Stewart JP, Seyhan E, Silva WJ, Chiou B-S-J, et al. NGA-West2 database. Earthq Spectra 2014;30:989–1005. https://doi.org/10.1193/070913EQS197M.
[7] Baker JW. Conditional mean spectrum: tool for ground-motion selection. J Struct Eng 2011;137:322–31. https://doi.org/10.1061/(ASCE)ST.1943-541X.0000215.
[8] Bradley BA, Burks LS, Baker JW. Ground motion selection for simulation-based seismic hazard and structural reliability assessment. Earthq Eng Struct Dyn 2015;44:2321–40. https://doi.org/10.1002/eqe.2588.
[9] Tarbali K, Bradley BA. Ground motion selection for scenario ruptures using the generalised conditional intensity measure (GCIM) method. Earthq Eng Struct Dyn 2015;44:1601–21. https://doi.org/10.1002/eqe.2546.
[10] Kohrangi M, Bazzurro P, Vamvatsikos D, Spillatura A. Conditional spectrum-based ground motion record selection using average spectral acceleration. Earthq Eng Struct Dyn 2017;46:1667–85. https://doi.org/10.1002/eqe.2876.
[11] Tsalouchidis KT, Moschen L, Adam C. Efficient selection of up to three-component ground excitation sets for earthquake engineering applications. Soil Dyn Earthq Eng 2021;148:106734. https://doi.org/10.1016/j.soildyn.2021.106734.
[12] Kayhan AH, Demir A, Palanci M. Multi-functional solution model for spectrum compatible ground motion record selection using stochastic harmony search algorithm. Bull Earthq Eng 2022;20:6407–40. https://doi.org/10.1007/s10518-022-01450-8.
[13] Mehdizadeh M, Mackie KR, Nielson BG. Scaling bias and record selection for quantifying seismic structural demand. J Struct Eng 2017:143. https://doi.org/10.1061/(ASCE)ST.1943-541X.0001855.
[14] Watson-Lamprey J, Abrahamson N. Selection of ground motion time series and limits on scaling. Soil Dyn Earthq Eng 2006;26:477–82. https://doi.org/10.1016/j.soildyn.2005.07.001.
[15] Tsalouchidis KT, Adam C. Amplitude scaling of ground motions as a potential source of bias: Large-scale investigations on structural drifts. Earthq Eng Struct Dyn 2022;51:2904–24. https://doi.org/10.1002/eqe.3707.
[16] Wen W, Ji D, Zhai C. Effects of ground motion scaling on the response of structures considering the interdependency between intensity measures and scale factors. Eng Struct 2020;209:110007. https://doi.org/10.1016/j.engstruct.2019.110007.
[17] Du W, Ning C, Wang G. The effect of amplitude scaling limits on conditional spectrum-based ground motion selection. Earthq Eng Struct Dyn 2019;48:1030–44. https://doi.org/10.1002/eqe.3173.
[18] Luco N, Bazzurro P. Does amplitude scaling of ground motion records result in biased nonlinear structural drift responses? Earthq Eng Struct Dyn 2007;36:1813–35. https://doi.org/10.1002/eqe.695.
[19] Roy R, Thakur P, Chakroborty S. Scaling of ground motions and its implications to plan-asymmetric structures. Soil Dyn Earthq Eng 2014;57:46–67. https://doi.org/10.1016/j.soildyn.2013.11.003.
[20] Reyes JC, González C, Kalkan E. Improved ASCE/SEI 7–10 ground-motion scaling procedure for nonlinear analysis of buildings. J Earthq Eng 2021;25:597–620. https://doi.org/10.1080/13632469.2018.1526140.
[21] Baker JW. Measuring bias in structural response caused by ground motion scaling. 8th Pacific Conference on Earthquake Engineering, Singapore: 2007, p. 1–8.
[22] Baker JW, Allin CC. A vector-valued ground motion intensity measure consisting of spectral acceleration and epsilon. Earthq Eng Struct Dyn 2005;34:1193–217. https://doi.org/10.1002/eqe.474.
[23] PEER GMSM Working Group. Evaluation of ground motion selection and modification methods: Predicting median interstory drift response of buildings. Berkeley, USA: 2009.
[24] Bradley BA. A generalized conditional intensity measure approach and holistic ground-motion selection. Earthq Eng Struct Dyn 2010:n/a-n/a. https://doi.org/10.1002/eqe.995.
[25] FEMA. Seismic performance assessment of buildings: volume 1 – methodology: FEMA P-58-1. Washington, D.C,: Federal Emergency Management Agency; 2018.
[26] Hatzigeorgiou GD, Liolios AA. Nonlinear behaviour of RC frames under repeated strong ground motions. Soil Dyn Earthq Eng 2010;30:1010–25. https://doi.org/10.1016/j.soildyn.2010.04.013.
[27] SAP2000 Integrated Software for Structural Analysis and Design n.d.
[28] Palanci M. Flexural response prediction of reinforced concrete members based on statistical observations. Arab J Sci Eng 2017;42:3689–709. https://doi.org/10.1007/s13369-016-2392-z.
[29] Demir A, Palanci M, Kayhan AH. Evaluation of supplementary constraints on dispersion of EDPs using real ground motion record sets. Arab J Sci Eng 2020;45:8379–401. https://doi.org/10.1007/s13369-020-04719-9.
[30] Palanci M, Kayhan AH, Demir A. A statistical assessment on global drift ratio demands of mid-rise RC buildings using code-compatible real ground motion records. Bull Earthq Eng 2018;16:5453–88. https://doi.org/10.1007/s10518-018-0384-y.
[31] Iervolino I, Maddaloni G, Cosenza E. Eurocode 8 compliant real record sets for seismic analysis of structures. J Earthq Eng 2008;12:54–90. https://doi.org/10.1080/13632460701457173.
[32] Dávalos H, Miranda E. Evaluation of bias on the probability of collapse from amplitude scaling using spectral-shape-matched records. Earthq Eng Struct Dyn 2019;48:970–86. https://doi.org/10.1002/eqe.3172.
[33] Gamst G, Meyers SL, Guarino AJ. Analysis of variance designs: a conceptual and computational approach with SPSS and SAS. 1st ed. Cambridge University Press; 2008.
[34] Kostinakis K, Athanatopoulou A, Morfidis K. Correlation between ground motion intensity measures and seismic damage of 3D R/C buildings. Eng Struct 2015;82:151–67. https://doi.org/10.1016/j.engstruct.2014.10.035.
[35] Palanci M, Senel SM. Correlation of earthquake intensity measures and spectral displacement demands in building type structures. Soil Dyn Earthq Eng 2019;121:306–26. https://doi.org/10.1016/j.soildyn.2019.03.023.
[36] Demir A. Investigation of the effect of real ground motion record number on seismic response of regular and vertically irregular RC frames. Structures 2022;39:1074–91. https://doi.org/10.1016/j.istruc.2022.03.091.
[37] Demir A, Palanci M, Kayhan AH. Probabilistic assessment for spectrally matched real ground motion records on distinct soil profiles by simulation of SDOF systems. Earthquakes and Structures 2021;21:395–411. https://doi.org/10.12989/eas.2021.21.4.395.

[38] Boore DM, Atkinson GM. Ground-motion prediction equations for the average horizontal component of PGA, PGV, and 5%-damped PSA at spectral periods between 0.01 *s* and 10.0 *s*. Earthq Spectra 2008;24:99–138. https://doi.org/10.1193/1.2830434.
[39] Campbell KW, Bozorgnia Y. A comparison of ground motion prediction equations for arias intensity and cumulative absolute velocity developed using a consistent database and functional form. Earthq Spectra 2012;28:931–41. https://doi.org/10.1193/1.4000067.
[40] Bommer JJ, Stafford PJ, Alarcon JE. Empirical equations for the prediction of the significant, bracketed, and uniform duration of earthquake ground motion. Bull Seismol Soc Am 2009;99:3217–33. https://doi.org/10.1785/0120080298.
[41] Akkar S, Sandıkkaya MA, Bommer JJ. Empirical ground-motion models for point- and extended-source crustal earthquake scenarios in Europe and the Middle East. Bull Earthq Eng 2014;12:359–87. https://doi.org/10.1007/s10518-013-9461-4.